

©2024 IEEE. This work has been submitted to the IEEE for possible publication. Copyright may be transferred without notice, after which this version may no longer be accessible.

Energy-Aware Dynamic Neural Inference

Marcello Bullo, *Student Member, IEEE*, Seifallah Jardak, Pietro Carnelli, Deniz Gündüz *Fellow, IEEE*

Abstract

The growing demand for intelligent applications beyond the network edge, coupled with the need for sustainable operation, are driving the seamless integration of deep learning algorithms into energy-limited, and even energy-harvesting end-devices. However, the stochastic nature of ambient energy sources often results in insufficient harvesting rates, failing to meet the energy requirements for inference and causing significant performance degradation in energy-agnostic systems. To address this problem, we consider an on-device adaptive inference system equipped with an energy-harvester and finite-capacity energy storage. We then allow the device to reduce the run-time execution cost on-demand, by either switching between differently-sized neural networks, referred to as multi-model selection (MMS), or by enabling earlier predictions at intermediate layers, called early exiting (EE). The model to be employed, or the exit point is then dynamically chosen based on the energy storage and harvesting process states. We also study the efficacy of integrating the prediction confidence into the decision-making process. We derive a principled policy with theoretical guarantees for confidence-aware and -agnostic controllers. Moreover, in multi-exit networks, we study the advantages of taking decisions incrementally, exit-by-exit, by designing a lightweight reinforcement learning-based controller. Experimental results show that, as the rate of the ambient energy increases, energy- and confidence-aware control schemes show approximately 5% improvement in accuracy compared to their energy-aware confidence-agnostic counterparts. Incremental approaches achieve even higher accuracy, particularly when the energy storage capacity is limited relative to the energy consumption of the inference model.

Index Terms

Intelligent processing, energy-aware deep learning, dynamic inference, energy harvesting, Markov decision process

This work received funding from the EU Horizon 2020 Marie Skłodowska Curie ITN Greenedge (GA. No. 953775), and UKRI through project SONATA (EPSRC-EP/W035960/1). For the purpose of open access, the authors have applied a Creative Commons Attribution (CC BY) license to any Author Accepted Manuscript version arising from this submission.

Marcello Bullo is with the Department of Electrical and Electronic Engineering, Imperial College London, and with Toshiba Bristol Research and Innovation Laboratory, Bristol (email: m.bullo21@imperial.ac.uk, marcello.bullo@toshiba-bril.com)

Seifallah Jardak and Pietro Carnelli are with Toshiba Bristol Research and Innovation Laboratory, Bristol (email: {name}.{surname}@toshiba-bril.com)

Deniz Gündüz is with the Department of Electrical and Electronic Engineering, Imperial College London (email: d.gunduz@imperial.ac.uk)

I. INTRODUCTION

The widespread presence of interconnected devices, driven by pervasive and ubiquitous computing paradigms, continuously generates an unprecedented volume of data. Machine learning (ML) and deep learning (DL) methodologies have demonstrated substantial efficacy in decoding patterns and extracting knowledge from heterogeneous sensor data [1], [2], enabling accurate predictions and informed decisions in many domains such as smart healthcare [3], [4], human activity recognition [5], [6], and intelligent transportation [7], [8]. However, energy and computational demands of DL models are typically prohibitive for practical deployment on mobile devices, characterized by limited computing power and constrained memory relative to dedicated servers. For example, in computer vision applications, state-of-the-art vanilla attention-based architectures, such as vision transformers, involve a number of parameters ranging from 86M to 632M [9], with the computational and memory cost of self-attention mechanism increasing quadratically with the image resolution [10].

Mobile edge computing (MEC) has emerged to bring intelligence closer to edge devices, [11] enhancing their computational capacity by offloading tasks to the network edge. Yet, its reliance on stable connectivity introduces trade-offs between latency and energy efficiency. In harsh channel conditions, offloading demands high transmit power, often exceeding the energy cost of local processing. This limitation underscores the need for an intelligent device-edge continuum [12], operating regardless of network quality [13]. In this scenario, energy-harvesting (EH) [14] can be pivotal in achieving energy-autonomy, and ensuring the sustainability and longevity of provided services, particularly those deployed in remote or inaccessible locations whereby regular battery replacement becomes unrealistic and cost-prohibitive [15].

A major challenge in the deployment of energy harvesting devices (EHDs) is the constrained and sporadic nature of the energy they capture. Therefore, while minimizing the energy consumption is the main goal in energy storage (ES)-operated devices in order to extend their lifespan, the primary objective with EHD is the intelligent management of available energy for prolonged operation. In principle, an EHD has access to a potentially infinite energy supply. However, this energy source is intermittent, requiring effective management to ensure stable operation and to mitigate the impacts of energy shortages. This involves developing strategies for dynamic adjustment of device activities based on energy availability.

Recent advancements in intermittent computing [13], [16] have enabled DL in EH IoT devices [17]–[21]. Traditional DL models are typically designed for environments with consistent energy sources and do not account for the stochastic availability of energy in EH scenarios. To address this, adaptive deep neural networks (DNNs) [22] can be employed. These models are capable of conditionally reducing the execution cost *on-demand* at inference time, trading-off performance with energy consumption. In general, in adaptive DNNs several computing modes are available for processing sensor data. Associated with each mode is an energy cost, with more costly modes generally yielding more reliable and accurate predictions.

We focus on two different techniques to implement adaptive inference under random energy dynamics: multi-model selection (MMS) [23]–[25] and early exiting (EE) [26]–[28]. MMS involves switching between different DNNs (computing modes), each with varying energy requirements, depending on the available energy. At the

Availability of feedback information		
Operational Granularity	Instance-Aware (IAw)	Instance Agnostic (IAg)
One-shot (OS)	OS-IAw-oracle	MMS
Incremental (Inc)	Inc-IAw-EE-DQN	Inc-IAg-EE

TABLE I: Summary of control methods studied in this paper.

beginning of the inference process, i.e., when a new sample arrives, the system selects one of the available DNNs conditioned on the current energy availability. Multi-exit networks incorporate multiple classifiers (computing modes) at different layers, enabling the inference task to terminate at an earlier stage if a decision is made to reduce the computational workload, thus skipping the subsequent layers. The adaptability of EE makes it particularly appealing for EH systems [20], [21], [29], [30], enabling design and run-time flexibility depending on the *availability of feedback information* in the decision-making process and the *operational granularity* of the action selection. When feedback information is available regarding the prediction confidence at the current exit branch, the system can amortize the instantaneous energy consumption by momentarily pausing or halting the computation pipeline if sufficient reliability in the current prediction is reached. We call this *instance-aware (IAw)* control. If no feedback information is available, then the decisions are based only on average (non-instantaneous) reliability metrics, e.g., accuracy on an unseen dataset available prior to deployment. This is referred to as *instance-agnostic (IAg)* control. By operational granularity we refer to the adaptivity of the EHD decision making process. When *incremental (Inc)* control is possible, a sequential decision process can be deployed, where the selection of an exit occurs progressively over time. Alternatively, *one-shot (OS)* control refers to a non-incremental approach, wherein the decision of a computing mode (exit branch or model) is made immediately upon the arrival of a sample. As a consequence, an Inc controller operates at a finer level than its OS counterpart, with the advantage of observing intermediate information and adjusting its action selection on-the-go.

In this paper, we focus on adapting neural inference workloads of EHDs to the available energy. The system adapts by implementing the specific adaptation strategy (either EE or MMS) contingent on the availability of feedback information and the operational granularity. Table I shows the control schemes resulting from the combination of such characteristics. EE, due to its incremental nature, allows for the integration of feedback information into the decision-making process, thereby enabling instance-aware (IAw) and incremental (Inc) control schemes. Conversely, MMS cannot function incrementally, as transitioning between models necessitates re-processing the current input instance from the initial input layer of the new model. Consequently, MMS operates exclusively in a OS manner, which precludes the integration of any feedback information into the decision-making process. Hence, the only MMS feasible controller is OS-IAg-MMS, which we simply refer to as MMS. Conversely, a OS-IAw controller is referred to as an *oracle* due to its impracticality, regardless of whether it pertains to EE or MMS. In the absence of feedback information in the decision-making process (IAg), OS-IAg-EE and MMS schemes are mathematically equivalent. Therefore, MMS is selected to represent OS-IAg controllers.

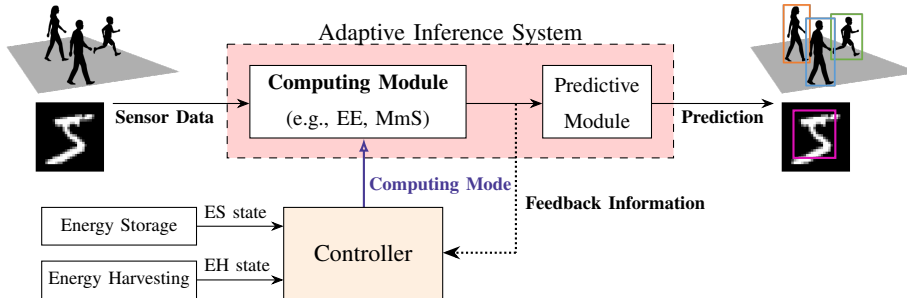


Fig. 1: System diagram of an adaptive inference system for resource-constrained devices. Sensor data are processed by a computing module (e.g., MMS or EE where the computation mode (e.g., model or exit selection), is regulated by the controller based on the ES level, EH dynamics, and potential feedback information (e.g., prediction confidence). In adaptive DNNs, the predictive module represents the sequence of operations converting the output likelihoods into the final prediction. In this scenario, the goal of the controller is to trade-off the prediction accuracy for the processing energy cost.

In the overall system depicted in Figure 1, we are concerned with the following fundamental question: how should inference in dynamic DNNs be optimized to deliver accurate predictions under stochastic availability of energy? Existing works predominantly focus on instance-agnostic short-term decision-making and heuristic approaches like policy networks and gating functions [22]. For instance, the model presented in [19] utilizes a single DNN implementing multi-resolution and EE to optimize energy usage. The exit selection relies on a lookup table of empirically measured charge times for short-term decisions. Similarly, the authors in [21] use an instance-agnostic reinforcement learning (RL)-based policy for exit selection. The approach in [30] implements runtime exit selection via an empirical joint threshold on the ES level and entropy of prediction likelihoods. These methods are mostly heuristic, and lack theoretical justifications. In contrast, our work addresses the energy-constrained inference problem from a theoretical perspective. A simpler scenario involving a DNN with one early exit is studied in our previous work [29]. Here, we delve into the generalized problem of optimal long-term scheduling of a finite number of computing modes, leveraging statistical information on EH. The problem is investigated for all the control schemes in Table I. The major contributions of this work are summarized as follows:

- We formulate the problem as a sequential decision problem promoting accurate predictions under uncertain energy dynamics by encoding the accuracy of the decisions into the reward signal.
- We establish the structure of the optimal policy for the MMS system, and show that it is monotone in the ES level;
- To have a principled upper-bound with theoretical guarantees for a multi-exit scheduler, we study a OS oracle controller which has full information of the per-instance exit confidences. We extend our previous analysis [29] to a more general case with a finite number of exits, characterizing the structure of the optimal policy.
- The optimal policy for the theoretical upper bound is based on the true, yet unknown, joint distribution of exit confidences. To numerically compute such a policy, we develop an approximate value iteration (VI) algorithm,

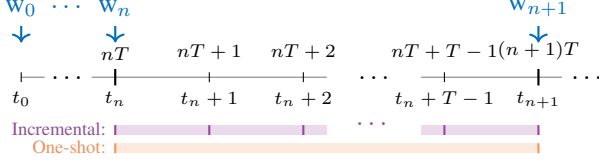


Fig. 2: Operational granularity of action selection.

which relies on the empirical distribution to estimate the expected value function in the Bellman equation. By leveraging the observed data, our method provides an effective approximation to the theoretical model.

- By addressing the EE selection as an instance-aware incremental control problem, we derive a sub-optimal policy using a Deep Q-Network (DQN) [31], referred to as Inc-I_{Aw}-EE.
- We also consider a OS-IAg system when the device is instance-agnostic, and empirically assess the benefits of instance-awareness and incremental decisions.
- We test and compare these systems on a custom multi-exit EfficientNet-based model [32] and TinyImageNet [33] dataset, by examining the resulting policies and analyzing the accuracy performance under different ES capacities and incoming energy rates.

The rest of the paper is organized as follows. Section II provides a detailed description of the system components, and a formal definition of the control schemes in Table I. In Section III, we formulate the optimization problem and establish the main theoretical results on optimal policies for the proposed controllers. Sections IV and V present the experimental setup and empirical results on the evaluation of our theoretical framework and comparison of the control schemes studied. Section VI concludes the article and discuss potential future directions. Detailed derivations, including proofs of theorems, are provided in Appendices.

II. SYSTEM MODEL

In this section, we begin with a description of the system model, outlining the key components of the proposed adaptive inference system. For clarity, Table II provides a summary of the main notation used in this work.

We formulate the problem as a discrete-time Markov decision process (MDP) with constant-duration time slots indexed by $t \in \mathbb{N}$. We assume that the sensing apparatus (e.g., a camera) monitors the environment at a constant rate, providing the resource-constrained device (RCD) with the instance w (e.g., an image) for processing every T slots. Without any loss of generality, we assume that the data arrival process starts at $t = 0$. Let $t_n = nT$, $n \in \mathbb{N}$, be the time index of the n -th data arrival. The controller selects the DNN model (MMS) or exit branch (EE) at which the computation is halted or temporarily paused, and operates at one of the two granularity levels: (1) singularly and responsively to the arrival of an input sample w , that is at decision epochs $\{t_n\}_{n \in \mathbb{N}}$, with an inter-action time of T slots (*one-shot*); or (2) incrementally within the interval $[t_n, t_{n+1})$, at intermediate time slots $t = t_n + \tau_t$, $\tau_t = 0, \dots, T-1$, $\forall n \in \mathbb{N}$ (*incremental*). Precisely, $\tau_t = t \bmod T$. The action selection scheme is depicted in Figure 2.

Notation	Definition
t	Time slot index
w_n	n -th random input
t_n	Arrival time index of w_n
K	Number of available computing modes
h_t	Energy Harvesting (EH) condition process at t
e_t^H	Energy harvested at t
b_{\max}	Energy Storage (ES) maximum capacity
$p_h^{h_i, h_j}$	$\mathbb{P}(h_{t+1} = h_j h_t = h_i)$
$p_{e^H}^h(e)$	$\mathbb{P}(e_t^H = e h_t = h)$
b_t	ES level at t
a_{t_n}	Action selected at t_n by a one-shot (Os) controller
α_t	Incremental sub-action (<i>pause/proceed</i>) selected at t
u_t	Energy cost of a_t , $u_t = u(a_t)$
ξ_t	Exit index at t (Incremental schemes)
τ_t	Processing stage at t (Incremental schemes)
z_t	Feedback information at t (prediction confidence)
$z_t^{(i)}$	i -th component of the feedback information at t
x_t	System state at t
s_t	Discrete component of the system state at t
$\hat{y}_{t_n}^{(k)}$	Prediction for w_n output by the k -th computing mode

TABLE II: Summary of used notations and their definitions.

Each action is selected based on the state of the stochastic process describing the EH dynamics and the ES level. Moreover, should the system consider a feedback information (IAw), prediction confidence can be accounted in the action selection. In the following sections we provide a detailed description of the mathematical models of each component.

A. Adaptive DNN Model

We define an adaptive DNN as $f(w; \theta)$, where $w \in \mathbb{R}^q$ and $\theta \in \mathbb{R}^d$ are the input and the trainable parameter vectors, respectively. Without loss of generality, f is considered as the composition of L differentiable operators l_i , $i = 1, \dots, L$, e.g., l_i represents a convolutional layer in a DNN. The final output is denoted as $\hat{y} = f(w; \theta)$. In a multi-exit DNN, let $K \leq L$ be the number of exit branches added to the NN structure. In order to provide a valid prediction at each exit branch, task-specific classifiers with comparatively negligible processing cost are required. We define the sub-network from the input layer to the k -th exit branch as $f(\cdot; \theta^{(k)})$, where $\theta^{(k)}$ represents the set of DNN parameters involved to the computation up to the k -th exit. Hence, $\hat{y}^{(k)} \triangleq f(w; \theta^{(k)})$ is the output at the k -th exit, and the final output is $\hat{y} = f(w; \theta^{(K-1)}) = \hat{y}^{(K-1)}$.

Similarly, in the MMS scenario, K refers to the different models $f_k(\cdot; \theta^{(k)})$, $k = 0, 1, \dots, K-1$ to be independently trained and deployed at the device. At the beginning of the inference process, the controller chooses one of the models to execute. We refer to each exit branch or model as a *computing mode*. Associated with the k -th mode is a fixed processing energy cost $u(f(\cdot; \theta^{(k)}))$, which, with a slight abuse of notation, is denoted as $u(k)$.

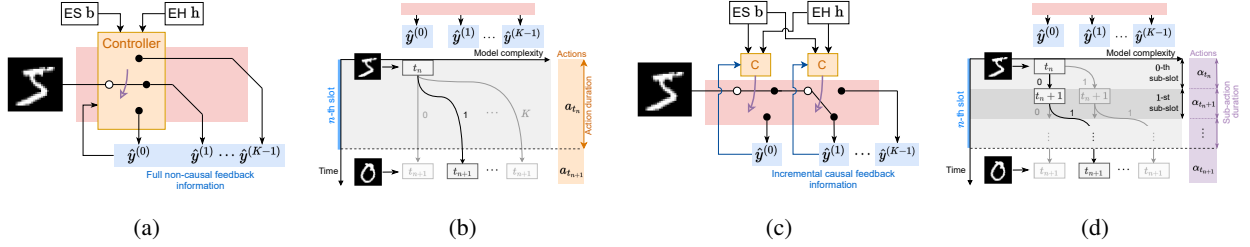


Fig. 3: Controlled computing modules defined by the granularity of action selection and the availability of feedback information. (a) and (b) depict the control scheme and an the temporal dynamics of an oracle OS-IAw controller, respectively. In the absence of feedback, this model reduces to the MMS scheme. Conversely, (c) and (d) represent Inc controls applicable to multi-exit networks: under causal feedback, the Inc-IAw-EE scheme is realized, whereas the absence of feedback yields the Inc-IAg-EE scheme.

Hence, processing modes that involve more parameters are more costly to perform, yet they output more reliable and accurate predictions. In this paper, we consider the 0-th computing mode as a random-guesser that outputs energy-free random predictions.

B. Energy Provision Model

We characterize the EH as a Markov-modulated process where $\mathbf{h}_t \in \mathcal{H} \triangleq \{h_1, \dots, h_{|\mathcal{H}|}\}$ describes the environment states, with transition probabilities $p_{\mathbf{h}}^{i,j} \triangleq \mathbb{P}(h_{t+1} = h_j | h_t = h_i)$. The energy $\mathbf{e}_t^H \in \mathcal{E}^H = \{e_1^H, \dots, e_{|\mathcal{E}_H|}^H\}$ provided by the harvesting circuit depends on environment state \mathbf{h}_t . Due to the uncertainty of environmental conditions, we model \mathbf{e}_t^H as a discrete random variable with probability mass function (pmf) $p_{\mathbf{e}^H}(e) \triangleq \mathbb{P}(\mathbf{e}_t^H = e | h_t = h)$, $e \in \mathcal{E}^H, h \in \mathcal{H}$. The harvested energy \mathbf{e}_t^H is used for the current inference task. Should \mathbf{e}_t^H exceed the computation energy demand u_t , the excess is stored in the ES, e.g., battery or supercapacitor. Conversely, if \mathbf{e}_t^H is insufficient for the task's demands, the deficit is compensated by drawing the necessary additional energy from the ES, when available. The ES is modeled as a discrete buffer of energy packets with finite capacity b_{\max} [34]–[36]. The energy level at time t is denoted by $\mathbf{b}_t = \{0, 1, \dots, b_{\max}\}$, and evolves according to

$$\mathbf{b}_{t+1} = \min\{[\mathbf{b}_t - \mathbf{u}_t + \mathbf{e}_t^H]^+, b_{\max}\}. \quad (1)$$

C. Instance-Aware Schemes

Instance-aware methods integrates the prediction confidence of an adaptive DNN as feedback within a closed-loop control scheme. We first describe an oracle OS-IAw controller having full information of the per-instance realizations of exit confidences. As mentioned in Section I, the theoretical derivations for OS-IAw fit both EE and MMS, since, mathematically, these two schemes are equivalent.

1) *One-Shot Instance-Aware (OsIAw) Controller (Oracle):* The one-shot controller operates every T slots, that is whenever a new instance w is provided by the sensor apparatus. Assuming that each EE step takes one time slot, it follows that $T \geq K - 1$. For $T \gg K - 1$, the time available for decision-making, thus for EH, is significantly

longer than the time required for the most computationally intensive mode. As a result, the system experiences fewer constraints. Conversely, when $T = K - 1$ the system is more constrained, as the time available for decision-making is reduced, leading to diminished EH within the decision epoch.

We model the problem as a discrete-time MDP $\langle \mathcal{X}, \mathbb{P}, \mathcal{A}, r \rangle$, with $t \in \mathbb{N}$ representing the time slot index, and $\mathcal{X}, \mathbb{P}, \mathcal{A}, r$ being the state space, the transition kernel, the action space and the reward, respectively. The decision epochs occur at time index t_n , and the controller adapts the computing mode (DNN model or exit branch) $a_{t_n} \in \mathcal{A} \triangleq \{0, \dots, K - 1\}$.

At time t_n , the state of the controller is defined as

$$\mathbf{x}_{t_n} = (\mathbf{s}_{t_n}, \mathbf{z}_{t_n}), \quad (2)$$

where $\mathbf{s}_{t_n} \triangleq (\mathbf{b}_{t_n}, \mathbf{h}_{t_n})$ is the joint energy level and environment state, with $\mathcal{S} = \mathcal{B} \times \mathcal{H}$, and \mathbf{z}_{t_n} encodes information about the DNN prediction quality for the current input instance. Ideally, $\mathbf{z}_{t_n} \in \{0, 1\}^K$ denotes the correctness vector, where index i contains a 1 if the prediction at the corresponding computing mode is correct. However, at inference time the true label y_{t_n} is unknown. Therefore, we define $\mathbf{z}_{t_n} \in [0, 1]^K$ as a measure of the vector of *correctness likelihoods* of DNN predictions, i.e., confidence levels. Precisely, our objective is for the i -th component of \mathbf{z}_{t_n} to represent the probability that the output prediction at the i -th computing mode is correct, given that its correctness likelihood estimate $g^{(i)}(\mathbf{w}_{t_n})$ is p , i.e.,

$$\mathbf{z}_{t_n}^{(i)} = \mathbb{P}(y_{t_n} = \hat{y}_{t_n}^{(i)} \mid g^{(i)}(\mathbf{w}_{t_n}) = p). \quad (3)$$

When the predictive module is a DNN, $g^{(i)}(\mathbf{w}_{t_n}) = \max_j f_j(\mathbf{w}_{t_n}; \theta^{(i)})$, where $f_j(\mathbf{w}_{t_n}; \theta^{(i)})$ is the j -th component of the softmax output of the DNN, and $\hat{y}_{t_n}^{(i)} = \arg \max_j f_j(\mathbf{w}_{t_n}; \theta^{(i)})$ is the predicted label. Moreover, if the DNN is perfectly calibrated, then $\mathbf{z}_{t_n}^{(i)} = g^{(i)}(\mathbf{w}_{t_n})$ [37], [38]. Therefore, we will adopt the per-instance confidences of a calibrated model as an estimate measure of the *correctness likelihoods* of DNN predictions. We assume that \mathbf{z}_{t_n} possesses a joint probability density function (pdf) $p_{\mathbf{z}}(\mathbf{z})$, $\mathbf{z} \in [0, 1]^K$, and that $\{\mathbf{z}_{t_n}\}_{n \geq 0}$ are independent and identically distributed (iid). Note that the latter assumption is a direct consequence of assuming that $\{\mathbf{w}_{t_n}\}_{n \geq 0}$ are iid, which is typical in machine learning applications for in-distribution instances.

Again, knowing \mathbf{z}_t for each new sample at the beginning of the slot requires the controller to have prior access to the confidences at all DNN computing modes, without paying the energy cost of running them. This is clearly unfeasible, thus we refer to such a controller as an *oracle*.

Note that at each decision epoch, the controller has access to \mathbf{b}_{t_n} and \mathbf{h}_{t_n} , but the value of \mathbf{e}_t^H is uncertain for future time instances $t = t_n, t_n + 1, \dots, t_{n+1} - 1$. Therefore, the controller lacks foresight regarding potential energy outages, and the action selection process must be constrained to guarantee $\mathbf{u}_{t_n} \leq \mathbf{b}_{t_n}$ and assure continuous operations. Formally, at each state \mathbf{x}_{t_n} the feasible action space is $\mathcal{A}_{\mathbf{x}_{t_n}} \triangleq \{a \in \mathcal{A} : \mathbf{u}(a) \leq \mathbf{b}_{t_n}\}$, where $\mathbf{u}(a)$ denotes the energy cost of a . For example, if the ES depletes ($\mathbf{b}_{t_n} = 0$), then only an energy-free random guess can be performed ($a_{t_n} = 0$), regardless of the harvested energy in the current slot. In general, the smaller b_{\max} , the more constrained the device is in its action selection process. Figures 3(a) and 3(b) illustrate the OS decision-making process with full non-causal feedback information.

The goal of a neural harvesting system is to continuously perform DNN-based inference under uncertain energy dynamics. When adaptive inference mechanisms (e.g., EE) are available, the goal is to accomplish inference tasks as accurately as possible while matching the energy constraints. To capture this behaviour, it is important that the reward encodes information on the performance of the system. Therefore, we define the reward function $r : \mathcal{S} \times \mathcal{Z} \times \mathcal{A} \rightarrow [0, 1]$ for the one-shot controller as the a_{t_n} -th component of the likelihood vector; that is, the correctness likelihood of the selected computing mode:

$$r(\mathbf{s}_{t_n}, \mathbf{z}_{t_n}, \mathbf{a}_{t_n}) = \mathbf{z}_{t_n}^{(a_{t_n})}. \quad (4)$$

2) *Incremental Instance-Aware (IncIAw) EE Controller*: To fully exploit the intrinsic incremental nature of EE while containing the limitations in the action selection of the one-shot oracle controller, we study a sequential decision scenario modeled as a discrete-time MDP $\langle \mathcal{X}_{\text{inc}}, \mathbb{P}_{\text{inc}}, \mathcal{A}^{\text{inc}}, r_{\text{inc}} \rangle$, where actions a_{t_n} are intended as incremental compositions of sub-actions.

The incremental controller operates in each slot t , where it chooses a sub-action α_t to decide whether to *pause* the computation and switching to idle mode, $\alpha_t = 0$, or *proceed* with the computation of the next exit, $\alpha_t = 1$. We denote the sub-action space as $\mathcal{A}^{\text{inc}} \triangleq \{0, 1\}$. The decision process starts with an energy-free random prediction (exit 0), and proceeds by incrementally choosing sub-actions α_t in subsequent slots. Every T slots, the computation for the current instance \mathbf{w}_{t_n} terminates, and the system becomes ready for a new sample $\mathbf{w}_{t_{n+1}}$. For example, in a DNN implementing $K = 3$ exits, setting $\alpha_{t_n} = 0$ corresponds to performing an energy-free random prediction in slot t_n . With $\alpha_{t_n+1} = 1$, the input instance is processed up to the first exit in the following slot $t_n + 1$, resulting in $a_{t_n} = 2$. Figures 3(c) and 3(d) illustrate the incremental decision-making process with causal feedback information.

At time t , the state of the controller is defined as

$$\mathbf{x}_t = (\mathbf{b}_t, \mathbf{h}_t, \xi_t, \tau_t, \mathbf{z}_t), \quad (5)$$

with $\mathbf{b}_t, \mathbf{h}_t$ being the ES and the EH processing states, $\xi_t = 0, \dots, K - 1$ representing the index of the current exit, $\tau_t = 0, \dots, T - 1$ denoting the processing stage of the current input, that is $\tau_t = t \bmod T$, and $\mathbf{z}_t \in [0, 1]$ representing the correctness likelihood of the current exit ξ_t . This can be expressed as the ξ_t -th component of the vector of correctness likelihoods introduced in Section II-C1, that is $\mathbf{z}_t = \mathbf{z}_{t_n}^{(\xi_t)}$. Therefore, conversely to the one-shot formulation, whereby the whole likelihood vector is known, in the incremental approach it can be revealed progressively as the computation proceeds, depending on the sub-actions selected. This makes the incremental approach feasible since the needed information is causal. As before, $\mathbf{s}_t = (\mathbf{b}_t, \mathbf{h}_t, \xi_t, \tau_t) \in \mathcal{S}_{\text{inc}}$ represents the discrete component of the state, and we refer to the set $\{t_n, t_n + 1, \dots, t_n + T - 1\}$ as the processing stage of the n -th input instance.

Although at the beginning of the n -th processing stage, the value of $\mathbf{e}_{t_n}^H$ is still uncertain, intermediate realizations \mathbf{b}_t and \mathbf{h}_t , $t = t_n + 1, \dots, t_n + K - 2$ can be observed, perhaps improving the estimation of future EH events and correcting the action selection on-the-go. This provides the controller with predictive insight into potential energy outages and overflow, enabling the execution of the i -th exit even when its total energy required to produce an output exceeds the amount of energy available when the computation started, i.e. \mathbf{b}_{t_n} . For example, in a system with

$K = 3$ exists and empty ES, i.e., $b_{t_n} = 0$, the one-shot controller is forced to select a random prediction. However, the incremental controller can switch to idle in the first slot and, in the case of sufficient energy provision, it can proceed further with the computation, potentially improving the quality of its prediction. Therefore, in each state \mathbf{x}_t the feasible action space is $\mathcal{A}_{\mathbf{x}_t}^{\text{inc}} \triangleq \{\alpha \in \mathcal{A}^{\text{inc}} : u_{\text{inc}}(\alpha, \mathbf{x}_t) \leq b_t\}$, where $u_{\text{inc}}(\alpha, \mathbf{x}_t)$ is the energy cost of α in state \mathbf{x}_t , specifically at exit ξ_t .

Similarly to the one-shot approach, the reward function $r_{\text{inc}} : \mathcal{S}_{\text{inc}} \times [0, 1] \times \mathcal{A}^{\text{inc}} \rightarrow [0, 1]$ is defined as

$$r_{\text{inc}}(\mathbf{s}_t, \mathbf{z}_t, \alpha_t) = \begin{cases} 0 & \text{for } \tau_t = 0, 1, \dots, T-2, \\ \mathbf{z}_{i(t)}^{(\xi_t + \alpha_t)} & \text{if } \tau_t = T-1 \end{cases},$$

where $i(t) = \lceil \frac{t}{K-1} \rceil$, with $\lceil \cdot \rceil$ representing the ceil rounding operator. In words, a null reward is collected for intermediate steps. At final slot $t_n - 1$, the reward is non-zero at the end of the n -th processing stage, where a decision is made by the controller.

D. Instance-Agnostic (IAg) Schemes

To assess the importance of taking actions based on the per-instance confidence values, we design both OS- and Inc-IAg controllers. These controllers operate over the identical state space as their IAw counterparts, but disregard the per-instance confidence values. We model the systems as discrete-time MDPs, where the state and action spaces are \mathcal{S} , \mathcal{A} and \mathcal{S}^{inc} , \mathcal{A}^{inc} , respectively. The performance of the k -th computing mode is measured by its prediction accuracy $\rho^{(k)}$, computed over a test dataset \mathcal{D} as

$$\rho^{(k)} \triangleq \frac{1}{|\mathcal{D}|} \sum_{i=1}^{|\mathcal{D}|} \mathbf{1}_{\{\hat{y}_i^{(k)} = y_i\}}, \quad (6)$$

where $\hat{y}_i^{(k)}$ and y_i denote the predicted label produced by the k -th mode, and the ground truth label, respectively, for the i -th input sample in \mathcal{D} . The rewards observed when action a , or sub-action α , is selected in state s , respectively, are:

$$r(s, a) = \rho^{(a)}, \quad (7)$$

$$r_{\text{inc}}(s, \alpha) = \begin{cases} 0 & \text{for } \tau = 0, 1, \dots, T-2, \\ \rho^{(\xi + \alpha)} & \text{if } \tau = T-1 \end{cases} \quad (8)$$

In words, when the k -th exit classifier is selected, the reward observed by the controller is the accuracy of the k -th classifier. Hence, IAg schemes use instance information from \mathcal{D} to compute $\rho^{(k)}$, but this estimate is fixed, and does not change as a function of the confidence of the current input instance, \mathbf{z}_t . Note that, when the DNN is perfectly calibrated, the reward received by selecting the k -th mode matches the mean confidence level of that classifier, that is $\rho^{(a)} = (1/|\mathcal{D}|) \sum_{i=1}^{|\mathcal{D}|} \mathbf{z}_i^{(a)}$.

E. Energy Considerations

Let $E^{(i)}$ denote the cumulative energy required for processing an input instance up to the i -th exit. Therefore, $E^{(1)} \leq E^{(2)} \leq \dots \leq E^{(K)}$. When an EE is selected, i.e., $a_{t_n} \neq K$, the task's energetic demand decreases,

$u_{t_n} < E^{(K)}$, and a reduced operating power can be used to accomplish the inference task by the end of the slot. In the case of an energy outage, i.e., $b_{t_n} - E^{(1)} + \sum_{\tau=0}^{T-1} e_{t_n+\tau}^H < 0$, none of the DNN executions are feasible, forcing an energy-free random guess of the current instance label. Conversely, in situations of energy overflow, $b_{t_n} - u_{t_n} + \sum_{\tau=0}^{T-1} e_{t_n+\tau}^H > b_{\max}$, the finite storage capacity of the ES prevents further energy accumulation, causing potential lost opportunities for future DNN executions.

III. SYSTEM OPTIMIZATION

Given an initial state x_0 , the goal is to find a one-shot stationary policy $\pi : \mathcal{S} \times \mathcal{Z} \times \mathcal{A} \rightarrow \mathcal{P}(\mathcal{A})$ and an incremental stationary policy $\pi_{\text{inc}} : \mathcal{S}_{\text{inc}} \times [0, 1] \times \mathcal{A}^{\text{inc}} \rightarrow \mathcal{P}(\mathcal{A}^{\text{inc}})$, which maximize the infinite-horizon discounted reward, that is

$$\pi^*(\mathbf{x}) = \arg \max_{\pi \in \Pi} \mathbb{E}_{\pi} \left[\sum_{n=0}^{\infty} \gamma^n r(\mathbf{x}_{t_n}, \mathbf{a}_{t_n}) \middle| \mathbf{x}_0 = \mathbf{x} \right], \quad (9)$$

$$\pi_{\text{inc}}^*(\mathbf{x}) = \arg \max_{\pi_{\text{inc}} \in \Pi_{\text{inc}}} \mathbb{E}_{\pi_{\text{inc}}} \left[\sum_{t=0}^{\infty} \gamma_{\text{inc}}^t r_{\text{inc}}(\mathbf{x}_t, \alpha_t) \middle| \mathbf{x}_0 = \mathbf{x} \right], \quad (10)$$

where γ is a discount factor. Specifically, in order for π^* and π_{inc}^* to be comparable, it must holds that $\gamma_{\text{inc}}^{t_{n+1}-1} = \gamma^n$ for all $n \in \mathbb{Z}_{\geq 1}$. This is because r_{inc} is non-zero only when $\tau_t = T-1$, that is $t = t_n + T-1 = t_{n+1} - 1, \forall n \geq 0$.

The following lemma shows the connection between the one-shot and the incremental approaches.

Lemma 1. *For any input instance w_{t_n} , and any specified action a_{t_n} , there exists a sequence of $K-1$ sub-actions $\{\alpha_{t_n+\tau}\}_{\tau=0}^{T-1}$ that would corresponds to $a_{t_n} \in \mathcal{A}$. Such correspondence can be expressed in closed-form as*

$$a_{t_n} = \sum_{\tau=0}^{T-1} \alpha_{t_n+\tau}.$$

Therefore, an optimal policy $\pi_{\text{inc}}^ : \mathcal{S} \times \Lambda \rightarrow \mathcal{P}(\Lambda)$ with respect to a generic objective in the incremental formulation is at least as good as an optimal policy for the same objective in the one-shot formulation $\pi^* : \mathcal{S} \times \mathcal{A} \rightarrow \mathcal{P}(\mathcal{A})$.*

As a consequence, the incremental approach offers a more fine-grained control strategy, ensuring performance at least as good as the one-shot alternative. In the next section, we characterize the structure of optimal policies for the OS-IAw controller and MMS, and we describe the DQN-based optimization of the Inc-IAw-EE controller.

A. Optimal Policy for the OS-IAw controller

In order to characterize the structure of the optimal policies we recall the definition of value-function and Q-function. The Bellman optimality equation for the svalue function is defined as

$$v^*(\mathbf{x}) = \max_{a \in \mathcal{A}_x} \mathbb{E}_{\mathbf{x}'} [r(\mathbf{x}, a) + \gamma v^*(\mathbf{x}')],$$

where $v^*(\mathbf{x}) \triangleq \max_{a \in \mathcal{A}_x} q^*(\mathbf{x}, a)$, and

$$q^*(\mathbf{x}, a) \triangleq \mathbb{E}_{\mathbf{x}'} [r(\mathbf{x}, a) + \gamma \max_{a' \in \mathcal{A}_x} q^*(\mathbf{x}', a')]. \quad (11)$$

Theorem 1 (Optimal value function). *The optimal value function for the OS-IAw controller is piece-wise linear in $\mathbf{z} \in \mathcal{Z}$*

$$v^*(\mathbf{s}, \mathbf{z}) = \sum_{j=0}^{K-1} \left(\mathbf{e}_j^\top \mathbf{z} + \gamma \sum_{\mathbf{s}' \in \mathcal{S}} \mathbb{P}(\mathbf{s}' | \mathbf{s}, a_j) \bar{v}^*(\mathbf{s}') \right) \mathbb{1}_{\{\mathbf{z} \in \mathcal{Z}_j(\mathbf{s})\}},$$

where $\bar{v}^*(\mathbf{s}) \triangleq \mathbb{E}_{\mathbf{z}}[v^*(\mathbf{s}, \mathbf{z})]$, and $\mathcal{P}_{\mathbf{s}} \triangleq \{\mathcal{Z}_j(\mathbf{s})\}_{j=0}^{K-1}$ forms a partition of \mathcal{Z} for each state $\mathbf{s} \in \mathcal{S}$. Moreover, the partition $\mathcal{P}_{\mathbf{s}}$ can be parameterized by at most $K-1$ real values, and can be expressed as

$$\mathcal{Z}_j(\mathbf{s}) = \{\mathbf{z} \in \mathcal{Z} : \mathbf{M}_j \mathbf{z} \geq \mathbf{F}_j \boldsymbol{\delta}(\mathbf{s})\}, \quad j = 0, \dots, K-1,$$

where $\boldsymbol{\delta}(\mathbf{s}) = [\delta_{0i}, i = 1, \dots, K-1] \in \mathbb{R}^{K-1}$ is a threshold vector with $\delta_{0i} = \gamma(\mathbb{P}_{a_0}(\mathbf{s}) - \mathbb{P}_{a_i}(\mathbf{s}))\bar{v}^*$, and $\mathbf{F}_j \in \{0, \pm 1\}^{K-1 \times K-1}$, $\mathbf{M}_j \in \{0, \pm 1\}^{K-1 \times K}$ are appropriate matrices.

As direct consequence of Theorem 1 we can state the following lemma.

Lemma 2 (Optimal policy). *The optimal policy π^* for the one-shot formulation is*

$$\pi^*(\mathbf{s}, \mathbf{z}) = \sum_{j=0}^{|\mathcal{A}_{\mathbf{s}}|-1} a_j \mathbb{1}_{\{\mathbf{z} \in \mathcal{Z}_j(\mathbf{s})\}}, \quad a_j \in \mathcal{A}_{\mathbf{s}}, \quad (12)$$

where $\mathbb{1}_{\{D\}}$ is the indicator function for event D .

The previous lemmas characterize the structure of the optimal value function, establishing that the one-shot optimal policy requires $|\mathcal{S}|$ partitions of \mathcal{Z} , $\mathcal{P}_{\mathbf{s}}$, each parameterized by $K-1$ values, say thresholds. This determines a finite structure, which is essential to design a value-iteration-based algorithm to compute ε -optimal policies. In fact, the algorithm can impose the optimal structure and iterate over a restricted set of policies, which contains the optimal ones. Such a structure simplifies when the 0-th exit classifier is a random predictor which outputs a random label for the current input instance. In this case, the 0-th entry of the confidence vector is constant, that is $z^{(0)} = 1/|\mathcal{Y}|$, where $|\mathcal{Y}|$ is the number of classes. This simplifies the structure of the optimal policy, providing a simpler geometrical interpretation.

Example 1 (OS-IAw with Initial Random Predictor). *Consider a DNN model implementing $K = 3$ computing modes, where the 0-th is a random predictor. The action space and the confidence vector are $\mathcal{A} = \{0, 1, 2\}$ and $\mathbf{z} = [1/|\mathcal{Y}|, z^{(1)}, z^{(2)}]$, respectively. In each state $\mathbf{s} = (b, h)$, the optimal value function is partitioned into $\{\mathcal{Z}_0(\mathbf{s}), \mathcal{Z}_1(\mathbf{s}), \mathcal{Z}_2(\mathbf{s})\}$, where $\boldsymbol{\delta}(\mathbf{s}) = [\delta_{01}(\mathbf{s}), \delta_{02}(\mathbf{s})]$ and*

$$\begin{aligned} \mathbf{M}_0 &= \begin{bmatrix} 1 & -1 & 0 \\ 1 & 0 & -1 \end{bmatrix}, \quad \mathbf{M}_1 = \begin{bmatrix} -1 & 1 & 0 \\ 0 & 1 & -1 \end{bmatrix}, \quad \mathbf{M}_2 = \begin{bmatrix} -1 & 0 & 1 \\ 0 & -1 & 1 \end{bmatrix}, \\ \mathbf{F}_0 &= \begin{bmatrix} -1 & 0 \\ 0 & -1 \end{bmatrix}, \quad \mathbf{F}_1 = \begin{bmatrix} 1 & 0 \\ 1 & -1 \end{bmatrix}, \quad \mathbf{F}_2 = \begin{bmatrix} 0 & 1 \\ -1 & 1 \end{bmatrix}. \end{aligned} \quad (13)$$

In particular, the equations describing $\mathcal{Z}_0(\mathbf{s})$,

$$z^{(1)} \leq \frac{1}{|\mathcal{Y}|} + \delta_{01}(\mathbf{s}), \quad \text{and} \quad z^{(2)} \leq \frac{1}{|\mathcal{Y}|} + \delta_{02}(\mathbf{s}) \quad (14)$$

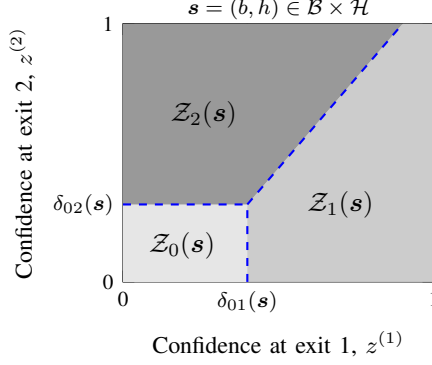


Fig. 4: Partition \mathcal{P}_s in the $z^{(1)}\text{-}z^{(2)}$ induced by the optimal value function with $K = 3$ exit classifiers.

defines a rectangular set in the $z^{(1)}\text{-}z^{(2)}$ plane, while for $\mathcal{Z}_1(s)$ and $\mathcal{Z}_2(s)$ we have

$$\mathcal{Z}_1(s) : \begin{cases} z^{(1)} \geq \frac{1}{|\mathcal{Y}|} + \delta_{01}(s) \\ z^{(1)} \geq z^{(2)} - \delta_{02}(s) + \delta_{01}(s), \end{cases}, \quad (15)$$

$$\mathcal{Z}_2(s) : \begin{cases} z^{(2)} \geq \frac{1}{|\mathcal{Y}|} + \delta_{02}(s) \\ z^{(1)} \leq z^{(2)} - \delta_{02}(s) + \delta_{01}(s) \end{cases}, \quad (16)$$

corresponding to a 45° separating line in the $z^{(1)}\text{-}z^{(2)}$ plane. Figure 4 visually represents the partition \mathcal{P}_s in $z^{(1)}\text{-}z^{(2)}$. Therefore, in state (s, z) , the optimal policy v^* selects action a_j whenever $z \in \mathcal{Z}_j(s)$.

In order to design an algorithm to find the optimal policy for the one shot controller, we restrict the search to policies with the structure described in Section III-A. Let

$$\Delta_{\mathbb{P}(s)} \triangleq [\mathbb{P}_{a_1}(s) - \mathbb{P}_{a_j}(s), j = 1, \dots, K-1].$$

Hence, $\delta^*(s) = \Delta_{\mathbb{P}(s)} \bar{v}^*$, and we rewrite $\bar{v}^*(s) = \mathbb{E}_z[v^*(s, z)]$ as

$$\bar{v}^*(s) = \sum_{j=0}^{K-1} \mathbb{E}_z \left[\left(e_j^\top z + \gamma \mathbb{P}_{a_j}(s) \bar{v}^* \right) \text{sgn}(\mathbf{M}_j z - \mathbf{F}_j(\Delta_{\mathbb{P}(s)} \bar{v}^*)) \right], \quad (17)$$

noting that $\bar{v}^*(s)$ is the fixed point of the following optimality operator

$$(\mathcal{T}\bar{v})(s) = \sum_{j=0}^{K-1} \mathbb{E}_z \left[\left(e_j^\top z + \gamma \mathbb{P}_{a_j}(s) \bar{v} \right) \text{sgn}(\mathbf{M}_j z - \mathbf{F}_j(\Delta_{\mathbb{P}(s)} \bar{v})) \right]. \quad (18)$$

Let \mathcal{T}^l be the composition of \mathcal{T} with itself l times. Since for discounted problems $\bar{v}(s) = \lim_{l \rightarrow \infty} (\mathcal{T}^l \bar{v})(s)$, $\forall s$ holds [39], value iteration (VI) can be used. However, applying \mathcal{T} requires the controller to know the joint distribution p_z , which is unknown. Therefore, at each iteration of VI, we approximate $\bar{v}(s)$ with the empirical-mean estimator $\hat{v}(s)$ computed over an estimation set $\mathcal{D}_{\text{est}} = \{z_i\}_{i=1}^D$.

This leads to the definition of an approximate optimality operator $\hat{\mathcal{T}}$ as follows

$$(\hat{\mathcal{T}}\bar{v})(s) = \frac{1}{D} \sum_{i=1}^D \sum_{j=0}^{K-1} \left(e_j^\top z_i + \gamma \mathbb{P}_{a_j}(s) \bar{v} \right) \text{sgn}(\mathbf{M}_j z_n - \mathbf{F}_j(\Delta_{\mathbb{P}(s)} \bar{v})). \quad (19)$$

Algorithm 1 ϵ -Approximate VI

Require: : $l = 0$, estimation set \mathcal{D}_{est} , $\bar{v}_0(\mathbf{s}) = 0, \forall \mathbf{s}$ **repeat**

$$\bar{v}_l(\mathbf{s}) = (\hat{\mathcal{T}}\bar{v}_{l-1})(\mathbf{s}), \forall \mathbf{s}$$

until $\|\bar{v}_l - \bar{v}_{l-1}\|_\infty \leq \epsilon$

Algorithm 1 described the ϵ -approximate VI which results in an ϵ -optimal \bar{v}_ϵ such that $\|\bar{v}_\epsilon - \hat{\bar{v}}\|_\infty \leq \epsilon$, whereby $\hat{\bar{v}} = \hat{\mathcal{T}}\hat{\bar{v}}$. Moreover, $\hat{\bar{v}}$ is an approximate solution of $\bar{v} = \mathcal{T}\bar{v}$, meaning that $\hat{\bar{v}} \approx \bar{v}^*$. Clearly, due to the strong law of large numbers, as the sample size $N \rightarrow \infty$, $\hat{\bar{v}} \rightarrow \bar{v}$ a.s., and an ϵ -optimal policy can be found. Otherwise, for finite N , an ϵ -sub-optimal policy will be obtained.

B. Suboptimal Policy for the Inc-IAw-EE

The incremental approach partitions each slot into non-empty disjoint sub-slots, where the controller chooses a sub-action to decide whether to switch to *idle mode*, or to *proceed* with the computation of the next exit. Unlike the one-shot formulation where z represents an uncontrollable state component, in the incremental scenario the evolution of z can be directly affected by the action α . Should the controller choose to proceed to the next exit, it will add further inference processing to the current input instance. Since the input of each layer of the model is the output of the previous layer, the sequential nature exhibits a Markovian property, whereby the future state is solely dependent on the current state. Therefore, given the state (\mathbf{s}, z) and the action α , the next state (\mathbf{s}', z') is determined as follows: \mathbf{s}' is generated according to $\mathbb{P}(\mathbf{s}'|\mathbf{s}, \alpha)$ and the next confidence value z' is generated according to the conditional probability $\mathbb{P}(z'|\mathbf{s}, z, \alpha)$. Note that the latter is unknown and, for each \mathbf{s} , it is a function of $z \in [0, 1]$. We could construct a model to learn these conditional probabilities, and design a model-based controller. However, optimizing separately the learning and the control problem may face extra costs without providing proportional performance benefits to the whole system. Therefore, we use DQN [31] to optimize the control problem without the explicit need for the approximation of the conditional distributions of confidence values $\mathbb{P}(\cdot|\mathbf{s}, z, \alpha)$.

DQN uses a neural network (NN), parameterized by θ , to approximate the optimal action-value function for all possible actions within a given state, that is $q_\theta^*(\mathbf{x}, a) \approx q^*(\mathbf{x}, a)$. At each time step t a replay buffer $R_t = \{e_i\}_{i=1}^t$ stores the agent's past experiences $e_t = (\mathbf{x}_t, a_t, r(\mathbf{x}_t, a_t), \mathbf{x}_{t+1})$ collected while interacting with the environment following an ϵ -greedy policy based on $q_{\theta_t}(\mathbf{x}, a)$. During learning, mini-batches of past experiences are sampled uniformly at random from R_t , and θ_t is updated minimizing [31]

$$\mathbb{E}_{(\mathbf{x}, \alpha, \mathbf{x}') \sim R_t} \left[(r(\mathbf{x}, \alpha) + \gamma \max_{\alpha'} q_{\tilde{\theta}_t}(\mathbf{x}', \alpha') - q_{\theta_t}(\mathbf{x}, \alpha))^2 \right]$$

through stochastic gradient descent. $\tilde{\theta}_t$ are the target network parameters which are periodically updated to mitigate correlations between the action and the target values.

Notably, the usage of a DNN-based approach to optimize the energy performance of another DNN may appear excessive. However, we use a lightweight fully-connected DNN to approximate the action-value function, described in Section IV-C.

C. Optimal Policy for the MMS controller

We characterize the optimal policy of MMS controller.

Theorem 2 (Optimality of monotone policies for MMS). *For the MMS problem, there exists a monotone non-decreasing optimal policy in the ES level $b \in \mathcal{B}$ of the form*

$$\pi_{MMS}^*(b, h) = \min\{a' : a' \in \arg \max_{a \in \mathcal{A}(b)} q_h^*(b, a)\}, \quad (20)$$

where $q_h^*(b, a)$ is the optimal Q -function for every $h \in \mathcal{H}$ as in (11).

Showing that the optimal policy for the MMS is monotone in the ES level has significant practical implications in developing efficient algorithms. Specifically, because the optimal solution reduces to identifying K thresholds on the ES level, a lookup table can be effectively stored on a resource-constrained device.

IV. EXPERIMENTAL SETUP

To validate our theoretical findings, we conducted simulation-based experiments. This section provides a comprehensive description of the architecture of DQN and the multi-exit DNN employed, including a detailed analysis of per-layer floating point operations (FLOPs), which underpins our rationale for implementing early exits within the architecture. Furthermore, we elaborate on the training methodology and calibration procedures employed, alongside the model and parameters used for the energy provision framework.

A. Dataset

In our experiments, we use a multi-exit DNN for image classification on Tiny Imagenet [33]. We partition the dataset into $\mathcal{D}_{\text{train}}$, $\mathcal{D}_{\text{cali}}$, \mathcal{D}_{est} and $\mathcal{D}_{\text{test}}$ as follows: $\mathcal{D}_{\text{train}}$ receives 70% of the data for the DNN training processes, $\mathcal{D}_{\text{cali}}$ is allocated 10% for calibration tasks, \mathcal{D}_{est} is assigned 10% to empirically estimate \hat{v} and learn the optimal policy, and the testing partition, $\mathcal{D}_{\text{test}}$, receives the remaining 10% of the data.

B. Multi-Exit EfficientNet: Design, Training and Calibration

We design multi-exit EfficientNet architectures based on EfficientNet-(B0-B7) models [32]. The exit classifier, attached at the end of each stage, is devised by replicating the structure of the final classifier, while adapting the input feature map size to match the output size of each stage. Detailed specifications of these exit classifiers are provided in Table III.

For each EfficientNet- Bm , we construct seven sub-networks $f_i(\cdot; \theta^{(m)})$, $i = 0, \dots, 6$, each formed by the composition of the first i -th stages and the exit classifier. We measure the computational cost, in terms of FLOPs for $f_i(\cdot; \theta^{(m)})$ to process an input instance from the Tiny ImageNet dataset. Figure 5 illustrates the computational cost in terms of FLOPs for multi-exit Efficientnet-B0 through Efficientnet-B4 relative to the stage index after which the exit classifier is attached. Intuitively, the increasing complexity from EfficientNet-B0 to EfficientNet-B4 is a consequence of compound scaling [32], which also results in higher FLOPs. Interestingly, for a given model m , the FLOPs do not always increase with the exit index i : due to the decreasing input resolution of each stage with

Network	Operator	Channels
Exit Classifier	MBConv4, k3x3	304
	Conv1x1	608
	BN & SiLU & Pooling & FC	200
Deep Q-Network	Fully Connected	64
	Fully Connected	64
	Fully Connected	2

TABLE III: Architecture of the exit classifier and DQN.

p_{eH}^G	p_{eH}^B	Energy Rate μ	Calibrated	Uncalibrated
			Accuracy %	Accuracy %
0.2	0.1	0.54	39.4	37.4
0.4	0.2	1.11	57.6	56.0
0.7	0.35	1.92	75.7	72.1
0.9	0.55	2.52	80.6	78.2
1	0.75	2.88	81.4	80.2
1	1	3.00	83.1	80.8

TABLE IV: The effect of calibration on the accuracy of OS-IAw controller. We set $b_{\max} = 5$, $p_G = 0.9$ and $p_B = 0.5$.

i. At earlier stages, the exit classifier has to process higher input resolution, which offsets the increase in channels and the number of layers per stage. For instance, for EfficientNet-B0 through EfficientNet-B2, attaching an exit classifier at the first stage is impractical because the resulting sub-network is shallower and requires more FLOPs than its subsequent stage.

In this study, we employ EfficientNet-B2 as the backbone model, augmented with an initial energy-free random predictor. Additionally, we introduce two early exits after the 3rd and 5th stages, resulting in a 4 multi-exit neural network. This selection is informed by the observation that the FLOPs required by these two early exits align with those of EfficientNet-B0 and EfficientNet-B1, as indicated by the dashed horizontal lines in Figure 5. Moreover, the cost in terms of FLOPs of the two early exits and the final one is approximately linear. To train the multi-exit EfficientNet on Tiny ImageNet [33], we formulate a joint optimization problem by aggregating the loss functions of the exit branches into a unified objective [26]. We adopt a similar training process as in [32], using Adam optimizer [40] with a learning rate of 1e-3, weight decay 1e-5 and momentum 0.9. The test set accuracies obtained by each exit classifier are 0.53, 0.69, 0.83, respectively. We perform temperature scaling calibration [37] to assure that the exit confidence of the classifiers is a representative estimate of the true likelihood.

C. Deep Q-Network

For the implementation of the incremental policy, the deep Q-network is designed as a compact fully connected DNN with two hidden layers of 64 neurons each. The total number of FLOPs is 6.6k, which represents only

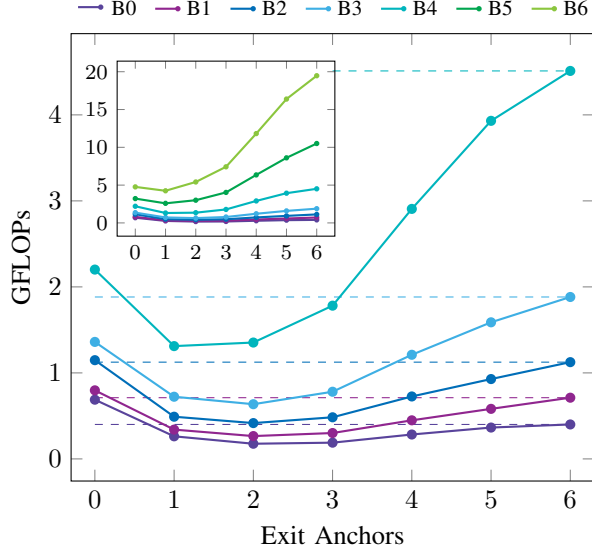


Fig. 5: FLOPs required to process an input instance for each sub-network $f_i(\cdot; \theta^{(i)})$, with i being the exit anchor, of the corresponding EfficientNet model. The inset picture shows the FLOPs for all EfficientNet models (from B0 to B6).

0.0017% of the computational complexity of EfficientNet-B0. The default hyperparameters are adopted from [31], except for the optimizer and learning rate which are sourced from [41].

D. Energy Harvesting (EH)

As outlined in Section II-B, we consider, without any loss of generality, a Markov chain with two environment states: (G)ood, and (B)ad, i.e., $\mathcal{H} = \{G, B\}$. These states signify favorable and unfavorable conditions, respectively. For instance, in the context of solar energy, the states could represent diurnal cycles of day and night or meteorological variations like sunny and cloudy conditions. Notice that the theoretical results derived in Section II hold for a generic Markov chain. Hence, a real EH source could be modeled better with additional environmental states. Nevertheless, it would also increase the complexity of the analysis unnecessarily.

For brevity, we define the transition probabilities as $p_h^G \triangleq p_h^{G,G}$ and $p_h^B \triangleq p_h^{B,B}$, $\forall t$. Similarly, the energy units harvested over a time slot are $e_t^H \in \{0, 1\}$ with $p_{e^H}^G \triangleq p_{e^H}^G(1)$ and $p_{e^H}^B \triangleq p_{e^H}^B(1)$, $\forall t$. The incoming energy rate generated by the EH process is defined as

$$\mu \triangleq p_G^\infty p_{e^H}^G + p_B^\infty p_{e^H}^B, \quad (21)$$

where p_h^∞ , $h \in \{G, B\}$, is the limiting distribution of the Markov chain $\{h_t\}$.

V. EXPERIMENTAL RESULTS

This section provides an extensive discussion of our experimental results. Section V-A investigates the impact of calibration on the decision-making performance under different energy constraints. In Section V-B, we numerically

derive and compare the policies for the controllers under study (listed in Table I). Specifically, we utilize Algorithm 1 to numerically obtain the ϵ -suboptimal policy for the OS-I_{Aw} oracle controller. For comparison, we also derive a model-free¹ oracle controller using DQN, referred to as OS-I_{Aw}-EE-oracle-DQN. The MMS policy, which is OS-I_{Ag}, is computed using policy iteration (PI). To assess the advantages of incremental controllers, we employ PI to compute an ϵ -optimal policy for the Inc-I_{Ag}-EE. Ultimately, DQN is used to derive the Inc-I_{Aw}-EE-DQN policy. In Section V-C, we conduct an extensive set of simulations to evaluate the long-term average accuracy (non-discounted) of the described models under different ES and EH conditions. This extensive testing enables us to compare the performance of our multi-exit DNN architectures across a range of operational scenarios, providing a robust assessment of their effectiveness and efficiency.

A. Calibrated vs Uncalibrated Oracle

We study the effect of calibration on decision-making performance of the oracle controller, i.e., OS-I_{Aw}. We select some representative values for the harvested energy pmf, where each corresponds to a different energy rate, therefore to a certain degree of energy constraint. We compute an ϵ -optimal policy through Algorithm 1 using an uncalibrated and a post-training calibrated DNN model. We measure the performance by the average number of correctly classified input samples in $\mathcal{D}_{\text{test}}$, computed for 200 episodes of length 100 steps. Table IV reports the parameters selected and shows the dominance of the calibrated DNN over its uncalibrated counterpart, with long-term average accuracy improvements varying between 1% and 3.6%. For this reason, in the remaining simulations we use calibrated DNNs.

B. Policy Comparison

We compare the numerical policies obtained for OS-I_{Aw}-oracle, MMS, Inc-I_{Ag}-EE and Inc-I_{Aw}-EE (DQN), using a discount factor of $\gamma = 0.9$, $b_{\max} = 30$, $p_h^B = 0.5$, $p_h^G = 0.9$, $p_{eH}^G = 0.8$, and $p_{eH}^B = 0$. As discussed in Section IV-B, we adopt a linearly increasing cost with the computation complexity. Precisely, the energy cost of the k -th computing mode is $u(k) = k$, $k = 0, 1, 2, 3$, where $k = 0$ refers to the initial random predictor.

All the policies we consider are deterministic, but they differ in their operational granularity. In fact, within the interval $[t_n, t_{n+1})$, the OS controller takes a single action to decide a computing mode while the Inc controller takes $T-1$ sub-actions to sequentially decide the optimal computing mode. Therefore, to compare the controllers' policies, we compute the fraction of input samples being processed at the k -th computing mode $\eta_k(b, h)$ when $b_{t_n} = b$ and $h_{t_n} = h$ at the beginning of each slot $[t_n, t_{n+1})$, $\forall n$. This can be interpreted as the empirical probability of selecting computing mode k in (b, h) .

In a given state (b, h) the MMS selection does not have any additional randomness, hence $\eta_k(b, h) = 1$ iff $k = \pi_{\text{MMS}}^*(b, h)$. Conversely, the OS-I_{Aw} (oracle) inherits the randomness from the input samples. Thus, we

¹By model-free we mean that the controller does not require the knowledge of the transition probabilities of the environment.

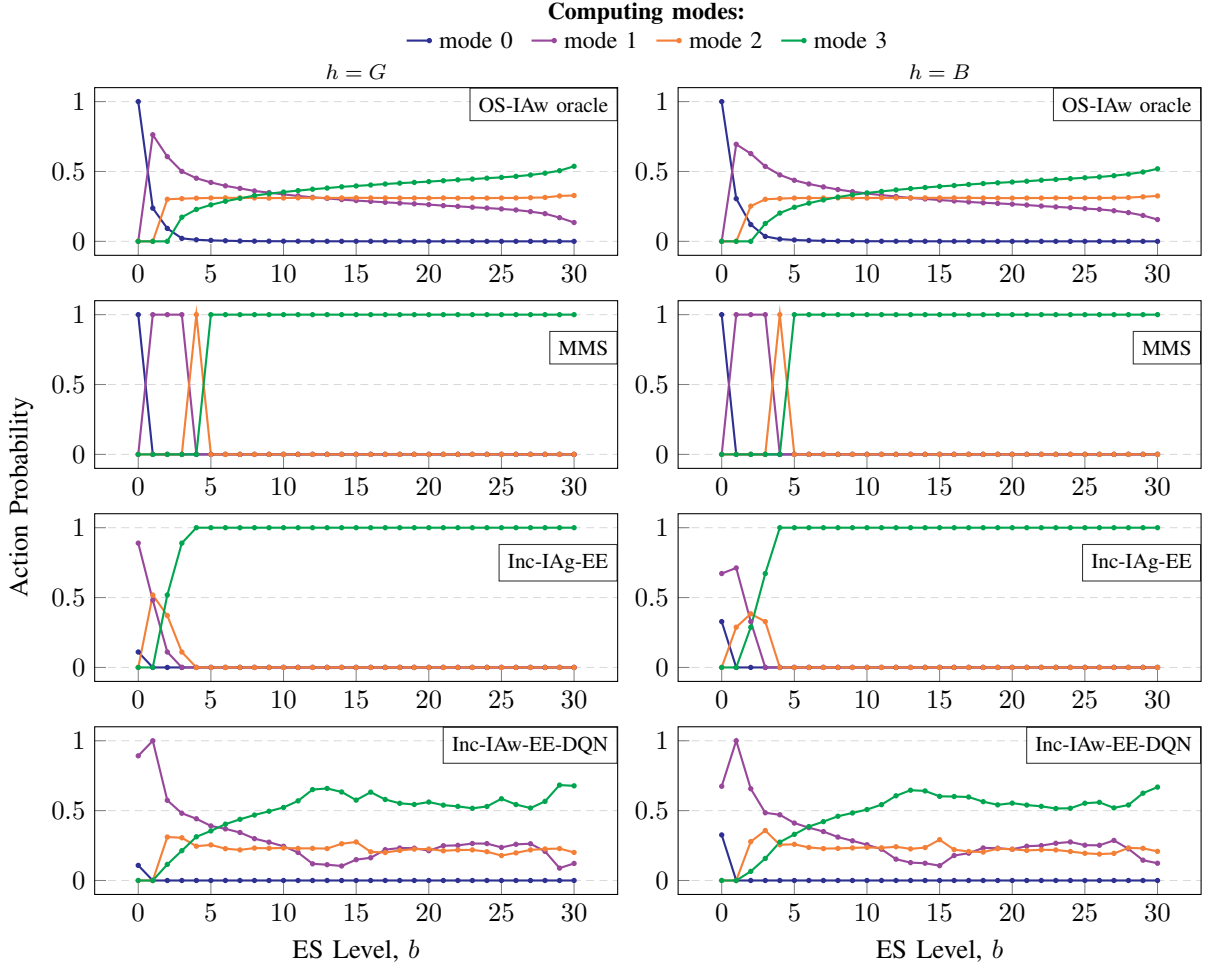


Fig. 6: Numerical policies expressed in terms of probability over the actions (y-axis) conditioned on the ES level (x-axis) and EH state (columns). Numerical values are computed for each controller with the appropriate algorithm using the following parameter setting: for $b_{\max} = 30$, $p_h^B = 0.5$, $p_h^G = 0.9$, $p_{eH}^G = 0.8$, $p_{eH}^B = 0$, $\gamma = 0.9$.

compute $\eta_k(b, h)$ as the fraction of samples in $\mathcal{D}_{\text{test}}$ being processed at the k -th mode when the controller follows π^* in (b, h) , that is

$$\eta_k(b, h) = \frac{1}{|\mathcal{D}_{\text{test}}|} \sum_{i=1}^{|\mathcal{D}_{\text{test}}|} \mathbb{1}_{\{z_i \in \mathcal{Z}_k(b, h)\}}. \quad (22)$$

For the Inc-IAg-EE controller, compared to the MMS one, the randomness stems from the intermediate energy arrivals which determine the evolution of b_t and h_t . So, we have

$$\eta_k(b, h) = \mathbb{P}\left(\sum_{\tau=0}^{T-1} \pi^*(b_{t_n+\tau}, h_{t_n+\tau}) = k \mid b_{t_n} = b, h_{t_n} = h\right).$$

A closed-form derivation is provided in Appendix VI. Finally, the Inc-IAw-EE (DQN) controller is instance-aware and incremental; hence, it is affected by both the randomness of input instances and intermediate energy arrivals.

To compute $\eta_k(b, h)$, we sample a sub-action trajectory $\Psi(b, h, z) = \{\alpha_\tau = \pi^*(\mathbf{b}_\tau, \mathbf{h}_\tau, \mathbf{z}^{(\tau)})\}_{\tau=0}^{T-1}$ such that $\mathbf{b}_0 = b$, $\mathbf{h}_0 = h$ and $\mathbf{z}_0 = z$. Hence,

$$\eta_k(b, h) = \frac{1}{|\mathcal{D}_{\text{test}}|} \sum_{i=1}^{|\mathcal{D}_{\text{test}}|} \mathbb{1}_{\left\{ \sum_{\alpha \in \Psi(b, h, z_i)} \alpha = k \right\}}. \quad (23)$$

Figure 6 shows the comparison in terms of computing mode (exit or model selection) probabilities for the policies of the four controllers mentioned above. The general trend indicates that the likelihood of selecting earlier exits (less energy-demanding models) increases as the ES level decreases. Conversely, deeper exits (more energy-demanding models) are preferred when the ES level is high. Moreover, we observe slightly less conservative policies when the computing mode is selected in (G)ood rather than (B)ad harvesting conditions. Such discrepancy is more noticeable for incremental controllers, where the action selection is optimized over a finer time granularity, thus more sensitive to modest energy variations.

1) *Comparing One-shot and Incremental Controllers:* Incremental approaches (Inc-IAg-EE, Inc-IAw-EE-DQN) are generally less conservative at low ES levels compared to one-shot methods (OS-IAw-oracle, MMS). For example, when $b = 0$, the MMS controller is restricted to selecting mode 0 (cost-free random predictor) as the ES is depleted. Instead, under the same conditions, the Inc-IAg-EE controller adopts a mixed strategy combining modes 0 and 1, despite $u(1) \geq 0$. Analogously, when $b = 1$, the Inc-IAg-EE controller operates by combining modes 1 and 2, in contrast to the MMS which conservatively opts for mode 1. In a similar manner, the Inc-IAw-EE-DQN policy enables the selection of mode 1 even when at the beginning of the decision epoch the ES is depleted. This flexibility is absent in the OS-IAw-oracle, where the cost-free random predictor remains the only feasible option.

Generally, one-shot controllers lack foresight of future energy realizations and thus optimizes on a time-averaged fashion within the slot. Conversely, incremental controllers operate at a finer granularity, and have more detailed information about intermediate EH conditions to take more informed decisions. In fact, an Inc controller waits for optimal EH conditions within the decision epoch duration and opportunistically selects later exits, potentially achieving better performance.

2) *Comparing Instance Agnostic and Instance Aware Controllers:* Instance-aware (OS-IAw-oracle, Inc-IAw-EE-DQN) controllers exhibit a more gradual transition between modes than their instance-agnostic counterparts (MMS, Inc-IAg-EE). For instance, although, OS-IAw-oracle is model-based and Inc-IAw-EE-DQN is model-free with more noisy mode probabilities, they both show a similar behaviour, starting with high probability for modes 0 and 1, and gradually shifting towards modes 2 and 3 as b increases. On the other hand, the MMS drastically switches between modes. Interestingly, at higher ES levels ($b \geq 5$) the most expensive mode (mode 3) becomes dominant for both instance-agnostic methods. This is because IAg controllers, lacking per-instance confidence, relies on average confidence, pushing for costly modes even when a less energy-intensive mode could yield good performance. This explains the IAw controller's strategy of processing only a fraction of input samples using the most energy-intensive mode when the ES is high, in favour of less energy-hungry modes with sufficient accuracy.

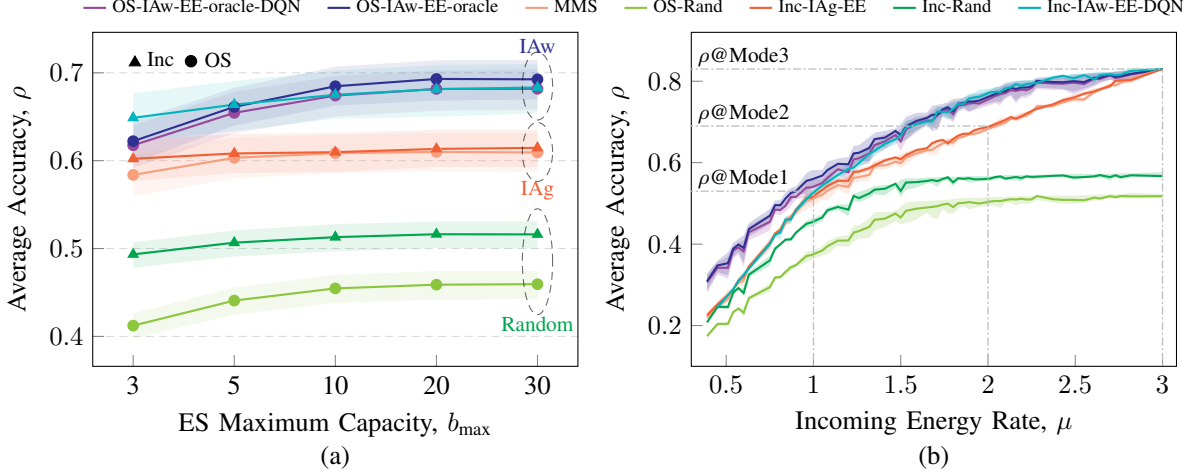


Fig. 7: (a) Average accuracy ρ_π computed as in (24) for each controller policy π as a function of the ES capacity b_{\max} . Triangle markers identify incremental methods, while circle markers the one-shot ones. (b) Average accuracy ρ_π as a function of the incoming energy rate μ computed as in (21).

C. Performance Comparison

This section provides a comprehensive comparison of various policies for EE and MMS under different energy conditions. Precisely, we compare the performance in terms of accuracy ρ_π accrued by the controller policy π continuously performing a classification task, that is

$$\rho_\pi \triangleq \frac{1}{T} \sum_{t_n=1}^T \mathbb{1}_{\{\hat{y}_{t_n}^{(a_{t_n})} = y_{t_n}\}} \mid a_{t_n} \sim \pi. \quad (24)$$

Each policy is obtained by solving a cumulative discounted reward problem with $\gamma = 0.9$. The accuracy is computed for 30 episodes of length $T = 5000$, using a combination of the following hyperparameters: $p_h^G \in \{0.5, 0.7, 0.9\}$, $p_h^B \in \{0.3, 0.5, 0.9\}$, $p_{eH}^G \in \{0.3, 0.7, 0.8, 1\}$, $p_{eH}^B \in \{0, 0.2, 0.3, 0.5\}$, and $b_{\max} = \{3, 5, 10, 20, 30\}$. For the analysis, we focus on the accuracy performance as function of the ES maximum capacity and the incoming energy rate.

1) *Average Accuracy versus b_{\max}* : Figure 7(a) illustrates the variation in the average accuracy achieved by the controller using a policy π in those environments (one for each combination of $p_h^G, p_h^B, p_{eH}^G, p_{eH}^B$) that have the same ES capacity b_{\max} . Generally, higher ES capacities with respect to the highest cost of the available modes lead to improved accuracy across all policies. A strategy based on random action selection underperforms compared to all the other methods that employ informed decision-making. Moreover, across all the ES capacities, IAw controllers consistently demonstrate higher accuracy than IAg ones, with performance improvements of up to 8% at large b_{\max} values. Notably, incremental approaches outperform one-shot counterparts at ES capacities comparable to the full-model energy requirements. In fact, the incremental controller can strategically delay its decision within the designated epoch, awaiting favorable EH conditions. This opportunistic strategy enables the selection of subsequent exits, which lead to enhanced performance. Indeed, the Inc-IAw-EE-DQN, which combines incremental decision-making and instance awareness, consistently dominates all the other policies in terms of accuracy when $b_{\max} \in \{3, 5\}$.

For higher values $b_{\max} \in \{10, 20, 30\}$, it even approaches the accuracy of OS-IAw-oracle, while matching that of OS-IAw-DQN. As a consequence, the small performance gap between OS-IAw-oracle and model-free controllers seems to represent the performance cost a system has to pay when the environment transitions are unknown (sub-optimality gap).

2) *Average Accuracy versus Incoming Energy Rate:* The environment model used in this paper is described by a significant number of parameters, i.e., $\{p_h^G, p_h^B, p_{eH}^G, p_{eH}^B, b_{\max}\}$. Each environment model is associated with an incoming energy rate μ , computed as in (21). Let U_μ be the set of environments with the same μ . The analysis in [29] shows that μ is not sufficient to summarize the whole behaviour of an environment: in general, for $u_1 \neq u_2$, $u_1, u_2 \in U_\mu$, the respective optimal policies $\pi^*(u_1)$ and $\pi^*(u_2)$ differ. However, we notice that the difference in performance between $\pi^*(u_1)$ and $\pi^*(u_2)$ is limited $\forall u \in U_\mu$. Therefore, we study the impact of the incoming energy rate μ on the controller performance ρ by computing the average accuracy over U_μ for the different rates μ , obtained from each combination of the parameters listed at the beginning of Section V-C.

Figure 7(b) displays the accuracy of different policies as a function of μ . We highlight in the plot the test accuracies of policies choosing always a fixed mode i , $\rho_{\text{Mode}i}$, and their minimum operating μ , corresponding to $\{(1, 0.53), (2, 0.69), (3, 0.83)\}$. As the incoming energy rate increases, as expected, the accuracy achieved by all the controllers improves. Random strategy underperforms compared to the informed methods. Moreover, across all the incoming energy rates, IAw policies consistently outperform IAg counterparts, with performance improvements reaching up to approximately 5%. Incremental approaches and their one-shot counterparts have comparable performance as a function of μ . To explain this, first note that under the same rate μ , the average amount of energy available over time is the same for both controllers. Moreover, for every input instance, Inc schemes optimize sub-action selection within a fixed horizon of T slots. Hence, waiting for better EH conditions comes at the cost of reducing the remaining time for computation. Therefore, the Inc schemes' advantage of exploiting frequent observations to adjust sub-actions in response to short-term state variations does not necessarily translate into significantly higher accuracy. This is especially the case when performance is measured by long-term average criteria, that can attenuate short-term stochastic variations.

The accuracy of IAg controllers exhibit a piece-wise linear structure as a function of μ , with breakpoints at $\mu = 1, 2$. Due to the unavailability of the per-instance confidence, these controllers always select the i -th computing mode when $\mu = u(i)$, and tend to linearly combine the frequency of using mode i and j , $i < j$, when $u(i) < \mu < u(j)$. Within the IAg controllers, MMS and Inc-IAg-EE behave similarly.

Instance-aware methods exploit the knowledge of per-instance confidence to push the performance beyond that of IAg controllers. The accuracy ρ as a function of μ is superlinear, with the maximum improvements of approximately 5% over IAg controllers reached around $\mu = 2$. At this rate, IAw methods achieve an accuracy of approximately 0.75 while IAg methods reach approximately 0.7. In general, for the same accuracy target, IAw controllers need lower incoming energy rates than their IAg counterparts. For example, the minimum energy rate required by IAw controllers to achieve an accuracy target equal to $\rho_{\text{Mode}2}$ is approximately 1.5, while for IAg ones it is 2. IAw methods dominate until the average incoming energy reaches 3 units per slot, which is enough to power the entire DNN. In this unconstrained scenario, the optimal behavior for all controllers is to consistently choose exit 3, which

has an energy cost of 3 and yields the highest accuracy. Overall, the OS-IAw-oracle controller (and similarly the OS-IAw-DQN-oracle) leads in performance, showing high accuracy even for incoming energy rates lower than the cost of the first computing mode ($u(1) = 1$). Particularly, for $0 \leq \mu < 1$, where the average available energy per slot is only sufficient to power a random-guesser, the instance-aware oracle controllers can leverage confidence information to achieve higher accuracy per unit of incoming energy. In the same energy rate range, the OS-IAw-DQN behaves as if confidence-awareness is not available, showing the same behaviour as IAg controllers.

D. Key Observations

Each policy can be interpreted as establishing dynamic thresholds for each computing mode, which vary with the ES level. For instance-aware methods, this dynamic nature is also influenced by the distribution of input confidences. Although the likelihoods produced by a DNN, even when calibrated, cannot be strictly considered as true probabilities, their integration into the decision-making process leads to more informed decisions, achieving higher accuracy with reduced energy consumption. This approach favors the selection of more energy-intensive modes only when necessary, such as when an input instance presents high complexity for the current task and DNN model. Furthermore, when a system with constrained b_{\max} operates in a low-incoming energy regime, incremental controllers outperform their one-shot counterparts. In our experiments, this is observed when the cost of the most expensive computing mode exceeds 60% of the system battery capacity b_{\max} . Instead, in high-incoming energy regimes, and for an unconstrained b_{\max} , the performance of one-shot and incremental controllers are comparable. In conclusion, if the distribution of input samples in the available dataset is statistically representative of the one in the user application, incorporating DNN output likelihoods into the decision-making process is recommended to enable instance-awareness. Additionally, our findings suggest that adopting multi-exit DNNs as a proxy for inference adaptation is advantageous, as it enables not only instance-awareness, but also incremental decision-making strategies with better performance with relatively small ES capacity.

VI. CONCLUSION AND FUTURE DIRECTIONS

In this paper, we addressed the challenges associated with adapting neural inference workloads to the available energy envelope and ES constraints in EHDs. We developed a comprehensive framework for optimal control in dynamic DNNs by studying MMS and EE strategies. These approaches were tailored to leverage instance-aware and instance-agnostic control schemes, operating at both one-shot and incremental granularities. Our main contributions include establishing the optimal policy structure for the MmS system, demonstrating its monotonicity in ES levels for energy and memory efficiency. We formulated a one-shot oracle controller using per-instance exit confidences with theoretical guarantees and designed an approximate VI algorithm to estimate optimal policies using empirical confidence distributions. Additionally, we developed a sub-optimal policy based on a lightweight DQN for incremental instance-aware EE selection, named Inc-IAw-EE. In conclusion, we conducted comprehensive empirical evaluations comparing our control schemes on a custom multi-exit EfficientNet model tested on the TinyImageNet dataset, analyzing accuracy under various ES capacities and energy rates. For the extensive range of parameter values examined in this work, simulations indicate that IAw and Inc control schemes can significantly enhance accuracy,

encouraging the adoption for practical designs. In fact, Inc approaches proved to be more efficient, achieving higher accuracy in scenarios with limited ES capacity, and IAw schemes consistently outperformed their IAg counterparts.

Future research can expand on several interesting directions. In many applications, collected data exhibits temporal correlations, which can be leveraged to decide the computing mode. While this paper assumes a sensing apparatus operating at a fixed sampling rate, a more general scenario involves input instances being collected at variable rates. In such cases, the intelligent management of time resources becomes essential. In fact, EE strategies can be employed to halt the processing earlier, thereby conserving both energy and time. This approach presents a significant trade-off between energy consumption and the time required for computation. However, effectively managing this trade-off necessitates a theoretical model for input arrivals, (e.g., a Poisson process).

APPENDIX A

Proof of Theorem 1. By definition of Bellman-optimal value function we have

$$\begin{aligned} v^*(\mathbf{s}, \mathbf{z}) &= \max_{a \in \mathcal{A}_s} \left\{ r(\mathbf{s}, \mathbf{z}, a) + \gamma \sum_{\mathbf{s}' \in \mathcal{S}} \mathbb{P}(\mathbf{s}'|\mathbf{s}, a) \int_{\mathcal{Z}} v^*(\mathbf{s}', \mathbf{z}') \mathbb{P}(\mathbf{z}') d\mathbf{z}' \right\} \\ &= \max_{a \in \mathcal{A}_s} \left\{ e_a^\top \mathbf{z} + \gamma \sum_{\mathbf{s}' \in \mathcal{S}} \mathbb{P}(\mathbf{s}'|\mathbf{s}, a) \bar{v}^*(\mathbf{s}') \right\}. \end{aligned} \quad (25)$$

By rewriting the above expression in a vector form, i.e., $\mathbb{P}_a(\mathbf{s}) \triangleq [\mathbb{P}(\mathbf{s}_1|\mathbf{s}, a), \dots, \mathbb{P}(\mathbf{s}_{|\mathcal{S}|}|\mathbf{s}, a)]^\top$, and $\bar{\mathbf{v}}^* = [\bar{v}^*(\mathbf{s}_1), \dots, \bar{v}^*(\mathbf{s}_{|\mathcal{S}|})]^\top$, we obtain

$$v^*(\mathbf{s}, \mathbf{z}) = \max_{a \in \mathcal{A}_s} \left\{ \mathbf{z}^{(a)} + \gamma \mathbb{P}_a^\top(\mathbf{s}) \bar{\mathbf{v}}^* \right\} = \max_{a \in \mathcal{A}_s} q^*(\mathbf{s}, \mathbf{z}, a) = \sum_{j=0}^{K-1} \left(e_j^\top \mathbf{z} + \gamma \mathbb{P}_{a_j}(\mathbf{s}) \bar{\mathbf{v}}^* \right) \mathbb{1}_{\{a_j \succeq a_i, \forall i \neq j\}}, \quad (26)$$

where $a_j \succeq a_i$ ² means that action a_j is at least as good as a_i in the following sense

$$a_j \succeq a_i \iff q^*(\mathbf{s}, \mathbf{z}, a_j) \geq q^*(\mathbf{s}, \mathbf{z}, a_i), \quad i \neq j. \quad (27)$$

By plugging the definition of q^* into (27) and re-arranging, we obtain $\forall i = 0, \dots, K-1$

$$z^{(a_j)} - z^{(a_i)} \geq \gamma (\mathbb{P}_{a_i}(\mathbf{s}) - \mathbb{P}_{a_j}(\mathbf{s})) \bar{\mathbf{v}}^*, \quad i \neq j. \quad (28)$$

Let $\delta_{ij}^*(\mathbf{s}) \triangleq \gamma (\mathbb{P}_{a_i}(\mathbf{s}) - \mathbb{P}_{a_j}(\mathbf{s})) \bar{\mathbf{v}}^*$. Note that

$$\delta_{ij}(\mathbf{s}) = -\delta_{ji}(\mathbf{s}), \quad (29)$$

$$\delta_{ij}(\mathbf{s}) = \delta_{ik}(\mathbf{s}) + \delta_{kj}(\mathbf{s}), \quad \forall i, j = 1, \dots, K. \quad (30)$$

Without loss of generality we choose a reference index, say $k = 0$. In this way, every $\delta_{ij}(\mathbf{s})$ can be rewritten as a function of δ_{0i} , $i = 0, \dots, K-1$, as follows:

$$\delta_{ij}(\mathbf{s}) = \delta_{i0}(\mathbf{s}) + \delta_{0j}(\mathbf{s}) \quad (31)$$

$$\delta_{ij}(\mathbf{s}) = -\delta_{0i}(\mathbf{s}) + \delta_{0j}(\mathbf{s}). \quad (32)$$

By definition (28), $\delta_{ii} = 0, \forall i$, therefore, $K-1$ values are sufficient to represent every $\delta_{ij}(\mathbf{s})$.

²Ties are broken arbitrarily.

According to (26), for each state $s \in \mathcal{S}$, \mathcal{Z} is partitioned into K subsets

$$\mathcal{Z}_j(s) = \{z \in \mathcal{Z} : M_j z \geq F_j \delta(s)\}, \quad j = 0, \dots, K-1,$$

where $\delta(s) = [\delta_{0i}, i = 1, \dots, K-1]$, $F_j \in \{0, \pm 1\}^{K-1 \times K-1}$ maps $\delta(s)$ into the corresponding thresholds according to (32), and $M_j \in \{0, \pm 1\}^{K-1 \times K}$ is a matrix formed by a negative identity matrix $-\mathbf{I}_{K-1}$ and a column vector of ones inserted at column index j . Therefore,

$$v^*(s, z) = e_j^\top z + \gamma \mathbb{P}_{a_j}(s) \bar{v}^*, \quad z \in \mathcal{Z}_j(s), \quad (33)$$

which is linear in $z \in \mathcal{Z}_j(s)$, $\forall j = 0, \dots, K-1$. \square

APPENDIX B

Proof of Theorem 2. We begin by characterizing the transition probabilities, where $\mathbb{P}(b', h' | b, h, a)$ indicates

$$\mathbb{P}(b_{t_{n+1}} = b', h_{t_n} = h' | b_{t_n} = b, h_{t_{n-1}} = h, a_{t_n} = a), \quad (34)$$

and $p_h(h' | h) \triangleq \mathbb{P}(h_{t_n} = h' | h_{t_{n-1}} = h)$, $\forall n \in \mathbb{N}$. Then, let $p_{b'}(b' | b, h, a) \triangleq \mathbb{P}(b_{t_{n+1}} = b' | b_{t_n} = b, h_{t_n} = h, a_{t_n} = a)$, where $b_{t_{n+1}} = \min([b_{t_n} - u(a_{t_n})]^+ + e_{t_n}^H, b_{\max})$, $\forall n \in \mathbb{N}$. Hence,

$$\begin{aligned} \mathbb{P}(b', h' | b, h, a) &= p_{b'}(b' | b, h', a) p_h(h' | h) \\ &= \sum_{e \in \mathcal{E}^H} \mathbb{1}_{\{b' = \beta(b, a, e)\}} p_h(h' | h) p_{e^H}^h(e | h'), \end{aligned}$$

where $\beta(b, a, e) \triangleq \min([b - u(a)]^+ + e, b_{\max})$.

For brevity, let $\mathbb{P}(e, h' | h) \triangleq p_h(h' | h) p_{e^H}^h(e | h')$, $v_h^*(b) \triangleq v_{\text{MMS}}^*(h, b)$, $\beta_{ij}^e \triangleq \beta(b_i, a_j, e)$ and $r_{ij} \triangleq r(b_i, a_j)$. In order for (20) to hold, it is sufficient to prove that

$$\begin{aligned} q_h^*(b, a) &= r(b, a) + \gamma \sum_{h' \in \mathcal{H}} \sum_{b'=0}^{b_{\max}} \mathbb{P}(b', h' | b, h, a) v_{h'}^*(b') \\ &= r(b, a) + \gamma \sum_{e, h'} \mathbb{P}(e, h' | h) v_{h'}^*(\beta(b, a, e)) \end{aligned} \quad (35)$$

has non-decreasing differences (superadditive) [42], that is for $b_2 \geq b_1$ and $a_2 \geq a_1$, $a_2, a_1 \in \mathcal{A}_{b_1}$,

$$q_h^*(b_2, a_2) - q_h^*(b_2, a_1) \geq q_h^*(b_1, a_2) - q_h^*(b_1, a_1). \quad (36)$$

Considering that the optimal value function v_h^* is the unique fixed point of $(\mathcal{T}v)(b) = \max_{a \in \mathcal{A}_b} q_h(b, a)$, i.e., $\lim_{\ell \rightarrow \infty} (\mathcal{T}^\ell v^0)(b) = v_h^*(b)$ for any arbitrary initial function v^0 , we show by means of an inductive argument over $\ell = 1, 2, \dots$ that (36) holds.

First, we note that for any ES level $b \in \mathcal{B}$ and feasible actions $a_1, a_2 \in \mathcal{A}_b$, the reward function has constant differences, that is

$$r(b, a_1) - r(b, a_2) = r(b^+, a_1) - r(b^+, a_2), \quad \forall b^+ \geq b. \quad (37)$$

Hence, for $v^0(b) = 0$, $\forall b$, (36) is satisfied since $q_h^0(b, a_2) - q_h^0(b, a_1) = 0$, $\forall b$. Assume that (36) holds for q_h^ℓ . Because of (37), this is equivalent to

$$\mathbb{E}_{e,h'} \left[v_{h'}^\ell(\beta_{22}^e) - v_{h'}^\ell(\beta_{21}^e) \right] \geq \mathbb{E}_{e,h'} \left[v_{h'}^\ell(\beta_{12}^e) - v_{h'}^\ell(\beta_{11}^e) \right].$$

Then

$$\begin{aligned} \delta_q^{\ell+1}(b_2) &= q_h^{\ell+1}(b_2, a_2) - q_h^{\ell+1}(b_2, a_1) \\ &= (r_{22} - r_{21}) + \gamma \mathbb{E}_{e,h'} \left[v_{h'}^\ell(\beta_{22}^e) - v_{h'}^\ell(\beta_{21}^e) \right] \\ &\geq (r_{12} - r_{11}) + \gamma \mathbb{E}_{e,h'} \left[v_{h'}^\ell(\beta_{12}^e) - v_{h'}^\ell(\beta_{11}^e) \right] \\ &= q_h^{\ell+1}(b_1, a_2) - q_h^{\ell+1}(b_1, a_1) = \delta_q^{\ell+1}(b_1) \end{aligned} \tag{38}$$

Therefore, since superadditivity of q_h is preserved through a Bellman update, q_h^* must be superadditive. \square

APPENDIX C EXIT PROBABILITY FOR INC-IAG-EE CONTROLLERS

Let us define the set of discrete states indicating that the system is at t -th processing stage as

$$\mathcal{S}_t \triangleq \{s = (b, h, \xi, \tau) \in \mathcal{S} : \tau = t\}.$$

We refer to \mathcal{S}_0 as the set of initial states. We allow $\tau = K - 1$ and we define a fictitious set of final states, \mathcal{S}_{K-1} , where the reward corresponding to the previously selected exit is accrued, and no actions are selected. Note that if $\tau = 0$ then $\xi = 0$, since the processing of an input instance always starts from the 0-th exit, therefore the number of initial states is $N_0 = |\mathcal{B}||\mathcal{H}|$ and the number of final states is $N_{K-1} = |\mathcal{B}||\mathcal{H}|K$. For every $s_0 \in \mathcal{S}_0$, we want to compute the probability of selecting the k -th exit in the remaining $K - 1$ slots, prior to the next sample arrival. Let π_{inc}^* the ε -optimal policy found by any dynamic programming algorithm, and $\mathbb{P}_{\pi_{inc}^*}$ the transition probability matrix induced by such policy. Without any loss of generality, we assume that the first N_0 states in $\mathbb{P}_{\pi_{inc}^*}$ are the initial states, indexed by $i = 0, \dots, N_0 - 1$. Similarly, the states indexed by $i = N_0, \dots, N_0 + N_{K-1} - 1$ are final states. Hence, the t -step transition probability matrix $\mathbb{P}_{\pi_{inc}^*}^{(t)}$, where for the n -th input instance, the time instant t corresponds to $t = t_n + t$, can be partitioned as follows

$$\mathbb{P}_{\pi_{inc}^*}^{(t)} = \begin{bmatrix} \mathbb{P}_{0,0}^{(t)} & \mathbb{P}_{0,K-1}^{(t)} & \mathbb{P}_{0,\tilde{s}}^{(t)} \\ \mathbb{P}_{K-1,0}^{(t)} & \mathbb{P}_{K-1,K-1}^{(t)} & \mathbb{P}_{K-1,\tilde{s}}^{(t)} \\ \mathbb{P}_{\tilde{s},0}^{(t)} & \mathbb{P}_{\tilde{s},K-1}^{(t)} & \mathbb{P}_{\tilde{s},\tilde{s}}^{(t)} \end{bmatrix},$$

where $\tilde{s} \notin \mathcal{S}_0$, $\tilde{s} \notin \mathcal{S}_{K-1}$, and, with a slight abuse of notation, we write $\mathbb{P}_{i,j}^{(t)} \triangleq \mathbb{P}^{(t)}(s' \in \mathcal{S}_j | s \in \mathcal{S}_i)$. In particular, we are interested in $\mathbb{P}_{0,K-1}^{(K-1)}$. Note that for every $0 < t \leq K - 1$, $\mathbb{P}_{0,0}^{(t)} = 0$, since for every $s \in \mathcal{S}_0$, $\tau_{t_n} = 0$ and, after t steps we have $\tau_{t_n+t} = \tau_{t_n} + t \neq 0$; if $t = K - 1$, $\mathbb{P}_{0,\tilde{s}}^{(K-1)} = 0$, since $\tau_{t_n+K-1} = \tau_{t_n} + K - 1 \neq 0$. Therefore, $\mathbb{P}_{0,K-1}^{(K-1)}$ is stochastic, since $\mathbb{P}_{\pi_{inc}^*}^{(K-1)}$ does. Finally, let the set of terminal states that end with exit k be

$$\mathcal{S}_{k,K-1} \triangleq \{s = (b, h, \xi, \tau) \in \mathcal{S} : \xi = k, \tau = K - 1\}.$$

The probability of choosing exit k whenever $s \in \mathcal{S}_0$, is

$$\eta_k(s) \triangleq \sum_{s' \in \mathcal{S}_{k, K-1}} \mathbb{P}_{\pi_{\text{inc}}^*}^{(K-1)}(s, s') = \mathbf{1}^\top \mathbb{P}_{0, K-1}^{(K-1)}(s),$$

where $\mathbb{P}_{0, K-1}^{(K-1)}(s)$ is the row of $\mathbb{P}_{\pi_{\text{inc}}^*}^{(K-1)}$ corresponding to s .

REFERENCES

- [1] L. Ren, Z. Jia, Y. Laili, and D. Huang, “Deep learning for time-series prediction in iiot: Progress, challenges, and prospects,” *IEEE Transactions on Neural Networks and Learning Systems*, pp. 1–20, 2023.
- [2] H.-C. Li, W.-S. Hu, W. Li, J. Li, Q. Du, and A. Plaza, “A3 clnn: Spatial, spectral and multiscale attention convlstm neural network for multisource remote sensing data classification,” *IEEE Transactions on Neural Networks and Learning Systems*, vol. 33, no. 2, pp. 747–761, 2022.
- [3] K. Muhammad, S. Khan, J. D. Ser, and V. H. C. d. Albuquerque, “Deep learning for multigrade brain tumor classification in smart healthcare systems: A prospective survey,” *IEEE Transactions on Neural Networks and Learning Systems*, vol. 32, no. 2, pp. 507–522, 2021.
- [4] S. Shukla and Neduncheliyan, “A review on machine learning methods in smart healthcare systems,” in *International Conference on Information and Communication Technology for Competitive Strategies*. Springer, 2022, pp. 325–335.
- [5] Y. Zhu, H. Luo, R. Chen, and F. Zhao, “Diamondnet: A neural-network-based heterogeneous sensor attentive fusion for human activity recognition,” *IEEE Transactions on Neural Networks and Learning Systems*, pp. 1–11, 2023.
- [6] K. Chen, L. Yao, D. Zhang, X. Wang, X. Chang, and F. Nie, “A semisupervised recurrent convolutional attention model for human activity recognition,” *IEEE Transactions on Neural Networks and Learning Systems*, vol. 31, no. 5, pp. 1747–1756, 2020.
- [7] Z. Zhou and H. Xu, “Decentralized adaptive optimal tracking control for massive autonomous vehicle systems with heterogeneous dynamics: A stackelberg game,” *IEEE Transactions on Neural Networks and Learning Systems*, vol. 32, no. 12, pp. 5654–5663, 2021.
- [8] Z. Wang, J. Zhan, C. Duan, X. Guan, P. Lu, and K. Yang, “A review of vehicle detection techniques for intelligent vehicles,” *IEEE Transactions on Neural Networks and Learning Systems*, vol. 34, no. 8, pp. 3811–3831, 2023.
- [9] A. Dosovitskiy, L. Beyer, A. Kolesnikov, D. Weissenborn, X. Zhai, T. Unterthiner, M. Dehghani, M. Minderer, G. Heigold, S. Gelly, J. Uszkoreit, and N. Houlsby, “An image is worth 16x16 words: Transformers for image recognition at scale,” in *International Conference on Learning Representations*, 2021. [Online]. Available: <https://openreview.net/forum?id=YicbFdNTTy>
- [10] L. Papa, P. Russo, I. Amerini, and L. Zhou, “A survey on efficient vision transformers: algorithms, techniques, and performance benchmarking,” *IEEE Transactions on Pattern Analysis and Machine Intelligence*, 2024.
- [11] Y. Mao, C. You, J. Zhang, K. Huang, and K. B. Letaief, “A survey on mobile edge computing: The communication perspective,” *IEEE communications surveys & tutorials*, vol. 19, no. 4, pp. 2322–2358, 2017.
- [12] H. Kokkonen, L. Lovén, N. H. Motlagh, A. Kumar, J. Partala, T. Nguyen, V. C. Pujol, P. Kostakos, T. Leppänen, A. González-Gil *et al.*, “Autonomy and intelligence in the computing continuum: Challenges, enablers, and future directions for orchestration,” *arXiv preprint arXiv:2205.01423*, 2022.
- [13] G. Gobieski, B. Lucia, and N. Beckmann, “Intelligence beyond the edge: Inference on intermittent embedded systems,” in *Proceedings of the Twenty-Fourth International Conference on Architectural Support for Programming Languages and Operating Systems*, ser. ASPLOS ’19. New York, NY, USA: Association for Computing Machinery, 2019, p. 199–213. [Online]. Available: <https://doi.org/10.1145/3297858.3304011>
- [14] D. Ma, G. Lan, M. Hassan, W. Hu, and S. K. Das, “Sensing, computing, and communications for energy harvesting iots: A survey,” *IEEE Communications Surveys & Tutorials*, vol. 22, no. 2, pp. 1222–1250, 2019.
- [15] H. N. S. Aldin, M. R. Ghods, F. Nayebipour, and M. N. Torshiz, “A comprehensive review of energy harvesting and routing strategies for iot sensors sustainability and communication technology,” *Sensors International*, p. 100258, 2023.
- [16] B. Lucia, V. Balaji, A. Colin, K. Maeng, and E. Ruppel, “Intermittent computing: Challenges and opportunities,” *2nd Summit on Advances in Programming Languages (SNAPL 2017)*, 2017.
- [17] M. Lv and E. Xu, “Deep learning on energy harvesting iot devices: Survey and future challenges,” *IEEE Access*, vol. 10, pp. 124 999–125 014, 2022.

- [18] Y. Zhao, S. S. Afzal, W. Akbar, O. Rodriguez, F. Mo, D. Boyle, F. Adib, and H. Haddadi, “Towards battery-free machine learning and inference in underwater environments,” in *Proceedings of the 23rd Annual International Workshop on Mobile Computing Systems and Applications*, 2022, pp. 29–34.
- [19] A. Montanari, M. Sharma, D. Jenkus, M. Alloulah, L. Qendro, and F. Kawsar, “eperceptive: energy reactive embedded intelligence for batteryless sensors,” in *Proceedings of the 18th Conference on Embedded Networked Sensor Systems*, ser. SenSys ’20. New York, NY, USA: Association for Computing Machinery, 2020, p. 382–394. [Online]. Available: <https://doi.org/10.1145/3384419.3430782>
- [20] Y. Li, Y. Wu, X. Zhang, E. Hamed, J. Hu, and I. Lee, “Developing a miniature energy-harvesting-powered edge device with multi-exit neural network,” in *2021 IEEE International Symposium on Circuits and Systems (ISCAS)*, 2021, pp. 1–5.
- [21] Y. Wu, Z. Wang, Z. Jia, Y. Shi, and J. Hu, “Intermittent inference with nonuniformly compressed multi-exit neural network for energy harvesting powered devices,” in *2020 57th ACM/IEEE Design Automation Conference (DAC)*, 2020, pp. 1–6.
- [22] Y. Han, G. Huang, S. Song, L. Yang, H. Wang, and Y. Wang, “Dynamic neural networks: A survey,” *IEEE Transactions on Pattern Analysis and Machine Intelligence*, vol. 44, no. 11, pp. 7436–7456, nov 2022.
- [23] R. Lee, S. I. Venieris, L. Dudziak, S. Bhattacharya, and N. D. Lane, “Mobisr: Efficient on-device super-resolution through heterogeneous mobile processors,” in *The 25th annual international conference on mobile computing and networking*, 2019, pp. 1–16.
- [24] S. Han, H. Shen, M. Philipose, S. Agarwal, A. Wolman, and A. Krishnamurthy, “Mcdnn: An approximation-based execution framework for deep stream processing under resource constraints,” in *Proceedings of the 14th Annual International Conference on Mobile Systems, Applications, and Services*, ser. MobiSys ’16. New York, NY, USA: Association for Computing Machinery, 2016, p. 123–136. [Online]. Available: <https://doi.org/10.1145/2906388.2906396>
- [25] R. A. Jacobs, M. I. Jordan, S. J. Nowlan, and G. E. Hinton, “Adaptive mixtures of local experts,” *Neural Computation*, vol. 3, no. 1, pp. 79–87, 1991.
- [26] S. Teerapittayanon, B. McDaniel, and H.-T. Kung, “Branchynet: Fast inference via early exiting from deep neural networks,” in *2016 23rd international conference on pattern recognition (ICPR)*. IEEE, 2016, pp. 2464–2469.
- [27] Y. Matsubara, M. Levorato, and F. Restuccia, “Split computing and early exiting for deep learning applications: Survey and research challenges,” *ACM Comput. Surv.*, vol. 55, no. 5, dec 2022. [Online]. Available: <https://doi.org/10.1145/3527155>
- [28] S. Scardapane, M. Scarpiniti, E. Baccarelli, and A. Uncini, “Why should we add early exits to neural networks?” *Cognitive Computation*, vol. 12, pp. 954 – 966, 2020. [Online]. Available: <https://api.semanticscholar.org/CorpusID:216553595>
- [29] M. Bullo, S. Jardak, P. Carnelli, and D. Gündüz, “Sustainable edge intelligence through energy-aware early exiting,” in *2023 IEEE 33rd International Workshop on Machine Learning for Signal Processing (MLSP)*, 2023, pp. 1–6.
- [30] Y. Li, Y. Wu, X. Zhang, J. Hu, and I. Lee, “Energy-aware adaptive multi-exit neural network inference implementation for a millimeter-scale sensing system,” *IEEE Transactions on Very Large Scale Integration (VLSI) Systems*, vol. 30, no. 7, pp. 849–859, 2022.
- [31] V. Mnih, K. Kavukcuoglu, D. Silver, A. A. Rusu, J. Veness, M. G. Bellemare, A. Graves, M. Riedmiller, A. K. Fidjeland, G. Ostrovski *et al.*, “Human-level control through deep reinforcement learning,” *nature*, vol. 518, no. 7540, pp. 529–533, 2015.
- [32] M. Tan and Q. Le, “Efficientnet: Rethinking model scaling for convolutional neural networks,” in *International conference on machine learning*. PMLR, 2019, pp. 6105–6114.
- [33] Y. Le and X. Yang, “Tiny imagenet visual recognition challenge,” *CS 231N*, vol. 7, no. 7, p. 3, 2015.
- [34] A. Nayyar, T. Başar, D. Teneketzis, and V. V. Veeravalli, “Optimal strategies for communication and remote estimation with an energy harvesting sensor,” *IEEE Transactions on Automatic Control*, vol. 58, no. 9, pp. 2246–2260, 2013.
- [35] N. Michelusi, K. Stamatou, and M. Zorzi, “On optimal transmission policies for energy harvesting devices,” in *2012 Information Theory and Applications Workshop*, 2012, pp. 249–254.
- [36] N. Jaggi, K. Kar, and A. Krishnamurthy, “Rechargeable sensor activation under temporally correlated events,” in *2007 5th International Symposium on Modeling and Optimization in Mobile, Ad Hoc and Wireless Networks and Workshops*, 2007, pp. 1–10.
- [37] C. Guo, G. Pleiss, Y. Sun, and K. Q. Weinberger, “On calibration of modern neural networks,” in *International conference on machine learning*. PMLR, 2017, pp. 1321–1330.
- [38] M. Minderer, J. Djolonga, R. Romijnders, F. Hubis, X. Zhai, N. Houlsby, D. Tran, and M. Lucic, “Revisiting the calibration of modern neural networks,” *Advances in Neural Information Processing Systems*, vol. 34, pp. 15 682–15 694, 2021.
- [39] D. Bertsekas and J. N. Tsitsiklis, *Neuro-dynamic programming*. Athena Scientific, 1996.
- [40] D. P. Kingma and J. Ba, “Adam: A method for stochastic optimization,” *arXiv preprint arXiv:1412.6980*, 2014.

- [41] A. Raffin, A. Hill, A. Gleave, A. Kanervisto, M. Ernestus, and N. Dormann, “Stable-baselines3: Reliable reinforcement learning implementations,” *Journal of Machine Learning Research*, vol. 22, no. 268, pp. 1–8, 2021. [Online]. Available: <http://jmlr.org/papers/v22/20-1364.html>
- [42] M. L. Puterman, *Markov Decision Processes: Discrete Stochastic Dynamic Programming*, 1st ed. USA: John Wiley & Sons, Inc., 1994.